

HF Skywave Massive MIMO Communication

Xianglong Yu¹, *Student Member, IEEE*, An-An Lu¹, *Member, IEEE*, Xiqi Gao¹, *Fellow, IEEE*,
Geoffrey Ye Li², *Fellow, IEEE*, Guoru Ding¹, *Senior Member, IEEE*, and Cheng-Xiang Wang¹, *Fellow, IEEE*

Abstract—In this paper, we investigate massive multi-input multi-output (MIMO) high frequency (HF) skywave communications. We first introduce a model for HF skywave massive MIMO channels within the orthogonal frequency division multiplexing transmission framework by using the matrix of sampled steering vectors. Considering the large antenna array aperture and increased signal bandwidth, the effect of the propagation delay across the large-scale antenna array cannot be ignored, and thus the steering vectors vary across different subcarriers. Specifically, we derive a wideband beam based channel model and show that the beam domain statistical channel state information (CSI) is frequency-independent. Then, we consider minimum mean-squared error (MMSE) based uplink receiver and downlink precoder with perfect CSI at the base station (BS). With a large number of antennas at the BS, the sum-rate can be asymptotically increased proportionally to the number of user terminals (UTs) while the transmit power per UT is scaled down inverse-proportionally to the number of antennas. In order to reduce the design complexities of the MMSE receiver and precoder, we derive a polynomial expansion based design using a deterministic equivalent. Simulation results demonstrate very significant performance advantages of the proposed HF skywave massive MIMO system.

Index Terms—Massive MIMO, HF skywave communications, channel model, receiver, precoder.

I. INTRODUCTION

TO ENABLE the global coverage for future wireless networks, satellite communication is an appealing can-

Manuscript received March 25, 2021; revised July 29, 2021 and September 19, 2021; accepted September 21, 2021. Date of publication October 5, 2021; date of current version April 11, 2022. This work was supported by the National Key R&D Program of China under Grant 2018YFB1801103, the National Natural Science Foundation of China under Grants 61801113, 61960206006, and 61971136, the Jiangsu Province Basic Research Project under Grant BK20195002, the Natural Science Foundation of Jiangsu Province under Grant BK20180362, and the Huawei Cooperation Project. The work of Guoru Ding was supported by the National Natural Science Foundation of China (No. U20B2038, No. 61871398), the Natural Science Foundation for Distinguished Young Scholars of Jiangsu Province (No. BK20190030). This article was presented at the IEEE GLOBECOM 2021 [1]. The associate editor coordinating the review of this article and approving it for publication was H. Q. Ngo. (Xianglong Yu and An-An Lu are co-first authors.) (Corresponding author: Xiqi Gao.)

Xianglong Yu, An-An Lu, Xiqi Gao, and Cheng-Xiang Wang are with the National Mobile Communications Research Laboratory, Southeast University, Nanjing 210096, China, and also with Purple Mountain Laboratories, Nanjing 211100, China (e-mail: xlyu@seu.edu.cn; aalu@seu.edu.cn; xqgao@seu.edu.cn; chxwang@seu.edu.cn).

Geoffrey Ye Li is with the Department of Electrical and Electronic Engineering, Imperial College London, London SW7 2AZ, U.K. (e-mail: geoffrey.li@imperial.ac.uk).

Guoru Ding is with the National Mobile Communications Research Laboratory, Southeast University, Nanjing 210096, China (e-mail: dr.guoru.ding@ieee.org).

Color versions of one or more figures in this article are available at <https://doi.org/10.1109/TWC.2021.3115820>.

Digital Object Identifier 10.1109/TWC.2021.3115820

didate technique and becomes a research hotspot [2], [3]. The high frequency (HF) band communications, usually using 3 to 30 MHz frequency band, enable over-the-horizon communications with ranges up to thousands of kilometers via ionospheric refraction, achieving global coverage without using expensive terrestrial and satellite infrastructures [4], [5]. Due to very limited spectrum resource and challenging ionospheric channel condition, HF communications usually have a low system rate, which have been at a disadvantage in competition with satellite communications. Aiming at increasing the system rate for HF communications, some works address the design of a multiple-input multiple-output (MIMO) architecture in recent years [6]–[9]. Most of the existing works can be categorized as point-to-point MIMO and a slight gain in the system rate can be achieved with small-scale MIMO (usually no more than 8 antennas) equipped in each end.

Massive MIMO deploys a large number of antennas at the base station (BS) to simultaneously serve multiple user terminals (UTs) and significantly improve the system sum-rate and reliability [10]. Furthermore, massive MIMO can provide the beamforming gain needed to overcome path loss and establish links with a reasonable signal-to-noise ratio [11]. Massive MIMO has become a critical technique for the fifth-generation wireless systems, and been widely investigated for the sub-6GHz band, mmWave/terahertz bands, and even optical band [12]–[14]. However, its application for the HF band is still missing in the literature. In this work, we apply massive MIMO for HF skywave communications, where the small angle spread is beneficial to separate multiple UTs from different directions. We consider a fixed BS equipped with a large-scale antenna array, serving a number of UTs, each with a single antenna.

We note that a large-scale antenna array at the HF band is implementable. A typical example is the HF skywave MIMO radar, where over a hundred antennas with a total length of over a thousand meters are employed in both the transmit and the receive arrays [15]. To the best of our knowledge, this is the first work in applying massive MIMO in the HF band in the literature. Thus, the widely used temporal-only HF channel models [16], [17] need to be extended to a model considering the spatial-temporal characteristics of the channels properly. Since the ionosphere is time-varying, a HF skywave communication system should adjust its carrier frequency accordingly [18], [19], which is different from terrestrial cellular communications.

Furthermore, when both the signal bandwidth and the array aperture are large, the propagation delay across the large-scale antenna array should not be ignored, which is referred to as the spatial-wideband effect and has been investigated in [12],

[20] for mmWave channels and in [21], [22] for terahertz channels more recently. The orthogonal frequency division multiplexing (OFDM) technique is very favorable for the wideband massive MIMO communications [10], and has been traditionally applied in wideband HF communications, even earlier than in cellular networks [23], [24]. In this paper, we first present a wideband massive MIMO-OFDM channel model for HF skywave communications by using the matrix of sampled steering vectors. Both the propagation delay and Doppler effect are considered in the wideband HF skywave massive MIMO channel model, and the matrix of the steering vectors varies with subcarriers due to the effect of the propagation delay across the large-scale antenna array. We will derive a wideband beam based channel model by using subcarrier-dependent sampled steering vectors and show that the statistical channel state information (CSI) in the beam domain is independent of subcarriers.

There generally exists two types of receivers and precoders for massive MIMO: nonlinear and linear ones. In this work, we focus on linear receiver and precoder to achieve a reliable performance with reasonable complexity for HF skywave massive MIMO communications. Among the existing linear receiver and precoder strategies, *e.g.*, maximal-ratio combining, zero-forcing, minimum mean-squared error (MMSE) criteria, the MMSE based receiver and precoder are proved to be near-optimal when the number of BS antennas is much larger than that of the single-antenna UTs [25]. It is well-known that the accuracy of CSI plays an essential role in massive MIMO communications. We consider the MMSE receiver and MMSE precoder for the uplink (UL) and downlink (DL) transmission, respectively, under the assumption that the channel is quasi-static and perfect DL CSI is available at the BS. The DL CSI can be obtained through UL training process and exploiting channel reciprocity in time-division duplex (TDD) mode. It may be challenging sometimes to obtain DL CSI at the BS. In this case, the robust DL precoder [14] can be applied for massive MIMO with imperfect DL CSI.

In general, the ergodic achievable sum-rates for the MMSE based receiver and precoder cannot be directly used to conduct the system performance analysis. The use-and-then-forget capacity bounding technique can provide closed-form lower bounds on ergodic sum-rate [10]. In this paper, we will alternatively derive closed-form asymptotic achievable sum-rate expressions under perfect CSI assumptions. We first prove that the scaled channel vectors of different UTs with non-overlapped directional cosines tend to be orthogonal when the number of BS antennas tends to infinity. The derived UL asymptotic achievable sum-rate and DL asymptotic achievable sum-rate approximation are only related to the statistical CSI and can be easily computed without expectation operation. We obtain the power-scaling law for the MMSE based UL and DL transmissions and show that the UL/DL sum-rates can be maintained and the transmit power can be significantly reduced when the BS is equipped with a sufficiently large number of antennas. Meanwhile, by simultaneously serving multiple UTs in the same time-frequency resource, the sum-rates can be proportionally increased compared with that of a single-antenna BS.

To avoid the computationally complex matrix inversion in calculating the MMSE based receiver and precoder, we also consider polynomial expansion (PE) based design for the UL receiver and DL precoder [26], [27]. The coefficient vectors of the PE based receiver and precoder are computed from the empirical moments of the channel Gram matrix, which need to be updated frequently once the channel changes, and the computations are still intensive. To further reduce the complexity, we turn to the deterministic equivalents of the empirical moments [28], [29]. Specifically, we derive a low-complexity design by computing the coefficient vectors based on the slow-varying statistical CSI and approximate them by their deterministic equivalents, which is independent of a particular channel realization.

The rest of this paper is organized as follows. In Section II, we introduce the system model for HF skywave massive MIMO communications. In Section III, we investigate the UL MMSE receiver and DL MMSE precoder, derive the asymptotic achievable sum-rate, and propose the low-complexity PE based design using deterministic equivalents. Simulation results are provided in Section IV, and Section V concludes this paper.

Notations: Boldface lower case letters and boldface upper case letters denote vectors and matrices, respectively. The operators $(\cdot)^H$, $(\cdot)^T$, and $(\cdot)^*$ represent the matrix/vector conjugate-transpose, transpose, and conjugate operations, respectively. \mathbf{I}_M is the $M \times M$ identity matrix. $\mathbf{0}$ and $\mathbf{0}_{M \times N}$ denote the zero vector and $M \times N$ zero matrix. The ensemble expectation, matrix trace, absolute value, Euclidean norm, and Frobenius norm operators are denoted by $\mathbb{E}\{\cdot\}$, $\text{tr}(\cdot)$, $|\cdot|$, $\|\cdot\|$, and $\|\cdot\|_{\mathbb{F}}$, respectively. $\text{diag}(\mathbf{A})$ indicates a column vector, which is constituted by the main diagonal of \mathbf{A} . \odot and $*$ denote the Hadamard product and convolution, respectively. $\bar{j} = \sqrt{-1}$. $[\mathbf{a}]_i$ and $[\mathbf{A}]_{i,j}$ denote the i -th element of \mathbf{a} , and the (i, j) -th element of \mathbf{A} , respectively. $\mathcal{CN}(\mathbf{a}, \mathbf{A})$ denotes the circular symmetric complex Gaussian distribution with mean \mathbf{a} and covariance \mathbf{A} . \sim denotes “be distributed as”. $\delta(\cdot)$ and $\delta[\cdot]$ denote the delta function and unit sample sequence, respectively. $\mathcal{P} \cup \mathcal{S}$ and $\mathcal{P} \cap \mathcal{S}$ denote the union and intersection operation of sets \mathcal{P} and \mathcal{S} , respectively. $E_j(x) = \int_1^{\infty} \frac{e^{-xt}}{t^j} dt$ is the generalized exponential integral function.

II. SYSTEM MODEL

In this section, we first introduce HF skywave massive MIMO communication and present the signal model within the OFDM framework. Then, we present a wideband HF skywave massive MIMO-OFDM channel model. Specifically, we derive a wideband beam based channel model and show the subcarrier-independent characteristic of the statistical CSI.

A. System Setup and Signal Model

We consider a long-range HF skywave massive MIMO communication system operating in TDD mode as illustrated in Fig. 1. The BS is equipped with a uniform linear array (ULA) consisting of M antennas and serves U single-antenna UTs. The ionosphere is divided into the D, E, and F

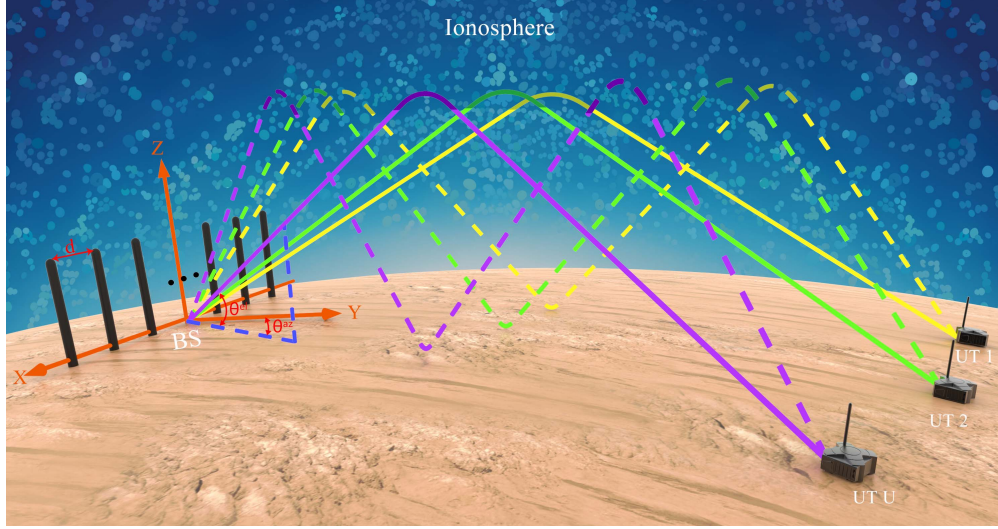


Fig. 1. Illustration of the HF skywave massive MIMO communication system.

layers. The E and F layers act mainly as radio wave reflectors, permitting long-range propagation, whereas the D layer acts principally as an absorber, causing signal attenuation [30]. Signal transmission over HF skywave channels can be characterized by multipath propagation. Specifically, the transmitted signal usually travels over multiple paths via single or multiple reflections from the E and/or F layers [31].

Let $x_u^{\text{ul}}(t)$ be the analog baseband signal transmitted by UT u . The received analog baseband signal vector at the BS is given by

$$\mathbf{y}^{\text{ul}}(t) = \sum_{u=1}^U \int_{-\infty}^{\infty} \mathbf{h}_u(t, \tau) x_u^{\text{ul}}(t - \tau) d\tau + \mathbf{z}^{\text{ul}}(t), \quad (1)$$

where $\mathbf{h}_u(t, \tau) \in \mathbb{C}^{M \times 1}$ is the time-varying UL channel impulse response vector from UT u to the BS, and $\mathbf{z}^{\text{ul}}(t)$ is the noise vector with M components being independent complex white Gaussian noise processes with identical power spectral density. Similarly, let $\mathbf{x}_u^{\text{dl}}(t) \in \mathbb{C}^{M \times 1}$ be the analog baseband signal vector transmitted for UT u . The received analog baseband signal at UT u is given by

$$y_u^{\text{dl}}(t) = \sum_{u'=1}^U \int_{-\infty}^{\infty} [\mathbf{h}_u(t, \tau)]^T \mathbf{x}_{u'}^{\text{dl}}(t - \tau) d\tau + z_u^{\text{dl}}(t), \quad (2)$$

where $[\mathbf{h}_u(t, \tau)]^T$ is the time-varying DL channel impulse response vector from the BS to UT u , expressed as the transpose of the UL channel impulse response vector according to the channel reciprocity [32], [33], and $z_u^{\text{dl}}(t)$ is the complex white Gaussian noise process.

Since the propagation distance difference between different paths is very large in HF skywave communications, large delay spread, up to milliseconds (ms), is usually observed [4]. There also exists Doppler shift introduced by the motion of both ionospheric layers and UTs [4], [34]. The HF skywave channel characteristics vary with the time of day, the seasons, the space weather, and the locations of the BS and UTs [18]. Typical ionosphere imposed Doppler spreads are 0.1 Hz, 0.5 Hz,

and 1 Hz for quiet, moderate, and disturbed ionospheric conditions at mid-latitude regions, respectively [31]. Besides, the modeling of the Doppler spread imposed by UT's mobility is similar to that in the terrestrial cellular communications. For example, if the UT is moving at the speed of 100 km/h and the carrier frequency is 16 MHz, the maximum Doppler spread is 1.48 Hz. In general, the channel coherence time, determined by the Doppler spread, is much larger than the channel delay spread. OFDM modulation has been used for the wideband HF skywave communication by adaptively selecting proper parameters [23], [35]. In the following, we focus on HF skywave massive MIMO communications with OFDM modulation.

Let N_c , N_g , and T_s be the number of subcarriers, the length of the cyclic prefix (CP), and the system sampling interval, respectively. We denote $T_c = N_c T_s$ and $T_g = N_g T_s$ the durations of the OFDM symbol and CP, respectively. We assume that N_v subcarriers, with index set $\mathcal{K} = \{0, 1, \dots, N_v - 1\}$, are used for transmitting data. The remaining $N_c - N_v$ virtual carriers are set as the guard band of the system, and the signals are set to 0 at these virtual carriers. Let $x_{u,\ell,k}^{\text{ul}}$ be the signal transmitted by UT u on the ℓ -th symbol at the k -th subcarrier. With the CP, the analog baseband signal on the ℓ -th symbol transmitted by UT u can be expressed as

$$x_{u,\ell}^{\text{ul}}(t) = \sum_{k \in \mathcal{K}} x_{u,\ell,k}^{\text{ul}} e^{j2\pi k \Delta f t}, \quad -T_g \leq t - \ell(T_c + T_g) < T_c, \quad (3)$$

where $\Delta f = 1/T_c$ denotes the subcarrier spacing. Similarly, let $\mathbf{x}_{u,\ell,k}^{\text{dl}} \in \mathbb{C}^{M \times 1}$ be the signal transmitted by the BS for UT u on the ℓ -th symbol at the k -th subcarrier. With the CP, the analog baseband signal vector on the ℓ -th symbol transmitted for UT u can be expressed as

$$\mathbf{x}_{u,\ell}^{\text{dl}}(t) = \sum_{k \in \mathcal{K}} \mathbf{x}_{u,\ell,k}^{\text{dl}} e^{j2\pi k \Delta f t}, \quad -T_g \leq t - \ell(T_c + T_g) < T_c. \quad (4)$$

We denote $\widehat{\mathbf{h}}_u(t, f)$ as the Fourier transform of $\mathbf{h}_u(t, \tau)$. The demodulated signal vector at the k -th subcarrier on the ℓ -th symbol at the BS can be written as

$$\mathbf{y}_{\ell,k}^{\text{ul}} = \sum_{u=1}^U \mathbf{h}_{u,\ell,k} \mathbf{x}_{u,\ell,k}^{\text{ul}} + \mathbf{z}_{\ell,k}^{\text{ul}}, \quad (5)$$

where $\mathbf{h}_{u,\ell,k} \in \mathbb{C}^{M \times 1}$ is the UL channel frequency response vector from UT u to the BS on the ℓ -th symbol at the k -th subcarrier, given by

$$\mathbf{h}_{u,\ell,k} = \widehat{\mathbf{h}}_u(\ell(T_c + T_g), k\Delta f), \quad (6)$$

and $\mathbf{z}_{\ell,k}^{\text{ul}}$ is the complex Gaussian noise vector distributed as $\mathcal{CN}(\mathbf{0}, \sigma_{\ell,k}^{\text{ul}} \mathbf{I}_M)$.

Similarly, the demodulated signal at the k -th subcarrier on the ℓ -th symbol at UT u can be written as

$$\mathbf{y}_{u,\ell,k}^{\text{dl}} = \sum_{u'=1}^U \mathbf{h}_{u,\ell,k}^T \mathbf{x}_{u',\ell,k}^{\text{dl}} + z_{u,\ell,k}^{\text{dl}}, \quad (7)$$

where $\mathbf{h}_{u,\ell,k}^T$ is the DL channel frequency response vector from the BS to UT u on the ℓ -th symbol at the k -th subcarrier, and $z_{u,\ell,k}^{\text{dl}}$ is the complex Gaussian noise distributed as $\mathcal{CN}(0, \sigma_{u,\ell,k}^{\text{dl}})$.

B. Channel Model

We consider a wide-sense stationary uncorrelated scattering channel model for HF skywave communications [16], [17], [36]. Let f_c denote the carrier frequency. Since the ionosphere is time-varying, the carrier frequency needs to be varied according to the real-time ionospheric conditions [18], [19]. Let d represent the inter-antenna spacing of the ULA. We define f_o as the maximum system operating frequency and set $d = \lambda_o/2$, where $\lambda_o = c/f_o$ is the wavelength corresponding to f_o and c is the speed of light.

We assume that there exist P_u resolvable paths between UT u and the BS. Let $\tau_{u,p,m}$ be the propagation delay of the p -th path between UT u and the m -th antenna of the BS, expressed as

$$\tau_{u,p,m} = \tau_{u,p,1} + (m-1)\Delta\tau \sin \theta_{u,p}^{\text{az}} \cos \theta_{u,p}^{\text{el}}, \quad (8)$$

where $\Delta\tau = d/c$, $\theta_{u,p}^{\text{az}}$ and $\theta_{u,p}^{\text{el}}$ are either the UL azimuth angle of arrival (AoA) and elevation AoA or the DL azimuth angle of departure (AoD) and elevation AoD associated with the p -th path, respectively. For notational convenience, we denote $\tau_{u,p} = \tau_{u,p,1}$ and $\Omega_{u,p} = \sin \theta_{u,p}^{\text{az}} \cos \theta_{u,p}^{\text{el}}$, and $\Omega_{u,p}$ can be referred to as the directional cosine with respect to the antenna array.

Angle spread is the result of the scattering of the signal during the reflections of the ionosphere and ground and also of the geometry of multipath propagation [34]. The azimuth AoA/AoD can differ from the great circle bearing from the BS to the UT, and an angle spread of about 1° is regarded as typical although larger spreads are sometimes observed under disturbed ionospheric conditions [30], [37], [38]. The elevation AoA/AoD depends upon the great circle ground range and which ionospheric modes are present [30]. The

observed elevation angle tends to lie within a small range for a long-range propagation [39].

The UL channel impulse response from UT u to the m -th antenna of the BS is given by

$$h_{u,m}(t, \tau) = \sum_{p=1}^{P_u} \alpha_{u,p}(t) e^{-j2\pi f_c(m-1)\Delta\tau\Omega_{u,p}} \delta(\tau - \tau_{u,p,m}), \quad (9)$$

where $\alpha_{u,p}(t)$ is a complex-valued gain random process. The p -th path is assumed to contain Q_p unresolvable subpaths with the same propagation delay, azimuth and elevation AoAs/AoDs since the surfaces of the earth and the ionospheric layers are rough [40]. Then, $\alpha_{u,p}(t)$ can be expressed as [41]

$$\alpha_{u,p}(t) = \sum_{q=1}^{Q_p} \beta_{u,p,q} e^{j\phi_{u,p,q}} e^{-j2\pi(f_c + \nu_{u,p,q})\tau_{u,p}} e^{j2\pi\nu_{u,p,q}t}, \quad (10)$$

where $\beta_{u,p,q}$, $\phi_{u,p,q}$, and $\nu_{u,p,q}$ are the gain, initial phase, and Doppler shift of the q -th subpath, respectively. We assume that $\phi_{u,p,q}$ is uniformly distributed over $[0, 2\pi)$. When Q_p tends to infinity, $\alpha_{u,p}(t)$ equals a complex Gaussian random process with zero mean. The amplitude of $\alpha_{u,p}(t)$ exhibits Rayleigh fading, which is widely confirmed in the HF skywave channel measurements [42], [43], and is a well-established characteristic adopted in the widely-used temporal-only HF channel models [16], [17].

For brevity, we express the UL channel impulse response vector from UT u to the BS as

$$\mathbf{h}_u(t, \tau) = \sum_{p=1}^{P_u} g_{u,p}(t, \tau) * \mathbf{g}(\Omega_{u,p}, \tau), \quad (11)$$

where

$$g_{u,p}(t, \tau) = \alpha_{u,p}(t) \delta(\tau - \tau_{u,p}), \quad (12)$$

$$\mathbf{g}(\Omega, \tau) = [g_1(\Omega, \tau), \dots, g_M(\Omega, \tau)]^T, \quad (13)$$

with

$$g_m(\Omega, \tau) = e^{-j2\pi f_c(m-1)\Delta\tau\Omega} \delta(\tau - (m-1)\Delta\tau\Omega). \quad (14)$$

Furthermore, according to (6), the UL channel frequency response vector can be derived as

$$\mathbf{h}_{u,\ell,k} = \sum_{p=1}^{P_u} \alpha_{u,p}(\ell(T_c + T_g)) e^{-j2\pi k\Delta f \tau_{u,p}} \mathbf{v}(\Omega_{u,p}, k), \quad (15)$$

where

$$\begin{aligned} \mathbf{v}(\Omega, k) &= \int_{-\infty}^{\infty} \mathbf{g}(\Omega, \tau) e^{-j2\pi k\Delta f \tau} d\tau \\ &= \left[1, e^{-j2\pi(f_c + k\Delta f)\Delta\tau\Omega}, \dots, e^{-j2\pi(f_c + k\Delta f)(M-1)\Delta\tau\Omega} \right]^T \end{aligned} \quad (16)$$

denotes the steering vector in the directional cosine of Ω at the k -th subcarrier. From (16), steering vector $\mathbf{v}(\Omega, k)$ varies with subcarriers. The spatial- and frequency-wideband has been

observed in mmWave massive MIMO systems [12], [20], and a physical channel model representing the overall spatial frequency channel matrix for a mmWave massive MIMO-OFDM system has been derived in [12], where the propagation delay across the array aperture is specifically focused. Differently, in the above physical channel model for our proposed HF skywave massive MIMO-OFDM system, both the propagation delay and Doppler effect are involved. In the following, based on the physical channel model in (15), we further derive a statistical channel model by using sampled steering vectors, which is referred to as the beam based channel model and will be used in the performance analysis of the UL receiver and DL precoder. We denote $\varphi_{u,p,\ell} = \alpha_{u,p}(\ell(T_c + T_g))$ for notational convenience, and $\varphi_{u,p,\ell}$ is a complex Gaussian random variable with zero mean.

We perform uniformly sampling for Ω . Let $\tilde{M} \geq M$ be the sampling number. We denote $\mathcal{S} = \mathcal{S}_1 \cup \dots \cup \mathcal{S}_{\tilde{M}} = (-1, 1]$ with $\mathcal{S}_{\tilde{m}} \in \left((2\tilde{m} - 2 - \tilde{M})/\tilde{M}, (2\tilde{m} - \tilde{M})/\tilde{M} \right]$ and $1 \leq \tilde{m} \leq \tilde{M}$, the overall directional cosine set. Let $\mathcal{P}_u = \{\Omega_{u,1}, \dots, \Omega_{u,P_u}\}$ be the directional cosine set of UT u . Then, $\mathbf{h}_{u,\ell,k}$ can be rewritten as

$$\mathbf{h}_{u,\ell,k} = \sum_{\tilde{m}=1}^{\tilde{M}} \sum_{\Omega_{u,p} \in \mathcal{P}_u \cap \mathcal{S}_{\tilde{m}}} \varphi_{u,p,\ell} e^{-j2\pi k \Delta f \tau_{u,p}} \mathbf{v}(\Omega_{u,p}, k). \quad (17)$$

Let $\gamma_{\tilde{m}} = (2\tilde{m} - 1 - \tilde{M})/\tilde{M}$ and the directional cosines of the paths in set $\mathcal{S}_{\tilde{m}}$ be approximated by $\gamma_{\tilde{m}}$. This approximation tends to be accurate when \tilde{M} tends to infinity. Then, $\mathbf{h}_{u,\ell,k}$ can be approximated as

$$\mathbf{h}_{u,\ell,k} = \sum_{\tilde{m}=1}^{\tilde{M}} \tilde{h}_{u,\ell,k,\tilde{m}} \mathbf{v}(\gamma_{\tilde{m}}, k), \quad (18)$$

where $\mathbf{v}(\gamma_{\tilde{m}}, k)$ is the sampled steering vector, and

$$\tilde{h}_{u,\ell,k,\tilde{m}} = \sum_{\Omega_{u,p} \in \mathcal{P}_u \cap \mathcal{S}_{\tilde{m}}} \varphi_{u,p,\ell} e^{-j2\pi k \Delta f \tau_{u,p}}. \quad (19)$$

The above channel approximation provides a beam based channel representation since the sampled steering vectors correspond to physical spatial beams. We refer to $\tilde{h}_{u,\ell,k,\tilde{m}}$ as beam domain channel coefficients, and $\tilde{h}_{u,\ell,k,\tilde{m}}$ is also complex Gaussian distributed with zero mean.

We denote $\tilde{\mathbf{h}}_{u,\ell,k} = [\tilde{h}_{u,\ell,k,1}, \dots, \tilde{h}_{u,\ell,k,\tilde{M}}]^T \in \mathbb{C}^{\tilde{M} \times 1}$, which is referred to as the beam domain channel vector from UT u to the BS at the k -th subcarrier on the ℓ -th symbol. We denote the matrix of the sampled steering vectors at the k -th subcarrier as

$$\mathbf{V}_k = [\mathbf{v}(\gamma_1, k), \dots, \mathbf{v}(\gamma_{\tilde{M}}, k)] \in \mathbb{C}^{M \times \tilde{M}}. \quad (20)$$

Then, we can rewrite (18) as

$$\mathbf{h}_{u,\ell,k} = \mathbf{V}_k \tilde{\mathbf{h}}_{u,\ell,k}, \quad (21)$$

which is similar to the channel representation presented for the terahertz band in [21].

Denote the channel coupling vector at the k -th subcarrier on the ℓ -th symbol as

$$\boldsymbol{\omega}_{u,\ell,k} = \mathbb{E} \left\{ \tilde{\mathbf{h}}_{u,\ell,k} \odot \tilde{\mathbf{h}}_{u,\ell,k}^* \right\} \in \mathbb{R}^{\tilde{M} \times 1}, \quad (22)$$

with the \tilde{m} -th element calculated by

$$\begin{aligned} [\boldsymbol{\omega}_{u,\ell,k}]_{\tilde{m}} &= \sum_{\Omega_{u,p} \in \mathcal{P}_u \cap \mathcal{S}_{\tilde{m}}} \mathbb{E} \left\{ |\varphi_{u,p,\ell}|^2 \right\} \\ &= \sum_{\Omega_{u,p} \in \mathcal{P}_u \cap \mathcal{S}_{\tilde{m}}} \sum_{q=1}^{Q_p} \beta_{u,p,q}^2. \end{aligned} \quad (23)$$

We can observe from (23) that the channel coupling vector is independent of symbols and subcarriers although the beam domain channel elements are related to symbols and subcarriers as shown in (19). Thus, we denote $\boldsymbol{\omega}_u = \boldsymbol{\omega}_{u,\ell,k}$ for brevity, which can be regarded as the statistical CSI.

III. MMSE BASED UL RECEIVER AND DL PRECODER

In this section, we investigate the MMSE based UL receiver and DL precoder. Specifically, we derive the asymptotic achievable sum-rate and analyze the power-scaling law, and propose low-complexity PE receiver and precoder based on deterministic equivalents.

A. UL Receiver and DL Precoder

We consider the MMSE based receiver and precoder by assuming perfect CSI at the BS. We focus on the transmission on the ℓ -th OFDM symbol. For brevity, we omit index ℓ in the subscript hereafter.

With the UL signal model in (5), the received signal vector at the k -th subcarrier at the BS is given by

$$\mathbf{y}_k^{\text{ul}} = \mathbf{H}_k \mathbf{x}_k^{\text{ul}} + \mathbf{z}_k^{\text{ul}}, \quad (24)$$

where $\mathbf{H}_k = [\mathbf{h}_{1,k}, \dots, \mathbf{h}_{U,k}] \in \mathbb{C}^{M \times U}$ is the UL channel matrix, \mathbf{x}_k^{ul} is the UL transmitted signal vector with $\mathbb{E} \{ \mathbf{x}_k^{\text{ul}} (\mathbf{x}_k^{\text{ul}})^H \} = q^{\text{ul}} \mathbf{I}_U$ where $[\mathbf{x}_k^{\text{ul}}]_u$ is the transmitted signal of UT u and q^{ul} is the average transmit power of each UT, and $\mathbf{z}_k^{\text{ul}} \sim \mathcal{CN}(\mathbf{0}, \sigma^{\text{ul}} \mathbf{I}_M)$ is the complex Gaussian noise vector.

Let $\mathbf{R}_k \in \mathbb{C}^{U \times M}$ denote the linear receiver. The MMSE receiver is obtained by solving the optimization problem of

$$\mathbf{R}_k^{\text{mmse}} = \arg \min_{\mathbf{R}_k} \mathbb{E} \left\{ \|\mathbf{x}_k^{\text{ul}} - \mathbf{R}_k \mathbf{y}_k^{\text{ul}}\|^2 \right\}. \quad (25)$$

We denote $\mathbf{G}_k = \mathbf{H}_k^H \mathbf{H}_k$ and $\rho^{\text{ul}} = q^{\text{ul}}/\sigma^{\text{ul}}$ for notational convenience. Then, we have

$$\mathbf{R}_k^{\text{mmse}} = \left(\mathbf{G}_k + \frac{1}{\rho^{\text{ul}}} \mathbf{I}_U \right)^{-1} \mathbf{H}_k^H. \quad (26)$$

With the DL signal model in (7), the received signal vector at the k -th subcarrier for a linearly precoded DL transmission can be expressed as

$$\mathbf{y}_k^{\text{dl}} = \mathbf{H}_k^T \mathbf{P}_k \mathbf{x}_k^{\text{dl}} + \mathbf{z}_k^{\text{dl}}, \quad (27)$$

where \mathbf{P}_k is the precoding matrix with power constraint $\text{tr} \{ \mathbf{P}_k^H \mathbf{P}_k \} \leq U$, \mathbf{x}_k^{dl} is the DL transmitted signal vector with $\mathbb{E} \{ \mathbf{x}_k^{\text{dl}} (\mathbf{x}_k^{\text{dl}})^H \} = q^{\text{dl}} \mathbf{I}_U$ where $[\mathbf{x}_k^{\text{dl}}]_u$ is the signal transmitted

for UT u and q^{dl} is the average transmit power for each UT, and $\mathbf{z}_k^{\text{dl}} \sim \mathcal{CN}(\mathbf{0}, \sigma^{\text{dl}} \mathbf{I}_U)$ is the complex Gaussian noise vector.

The MMSE precoder is obtained by solving the optimization problem of

$$\begin{aligned} \mathbf{P}_k^{\text{mmse}} &= \arg \min_{\mathbf{P}_k} \mathbb{E} \left\{ \|\mathbf{x}_k^{\text{dl}} - \zeta_k \mathbf{y}_k^{\text{dl}}\|^2 \right\}, \\ \text{s.t. } \text{tr}(\mathbf{P}_k^H \mathbf{P}_k) &\leq U, \end{aligned} \quad (28)$$

where ζ_k is a real scalar parameter corresponding to the potential power scaling performed at the UTs. Then, we have

$$\mathbf{P}_k^{\text{mmse}} = \frac{1}{\zeta_k^{\text{mmse}}} \left(\left(\mathbf{G}_k + \frac{1}{\rho^{\text{dl}}} \mathbf{I}_U \right)^{-1} \mathbf{H}_k^H \right)^T, \quad (29)$$

where $\rho^{\text{dl}} = q^{\text{dl}}/\sigma^{\text{dl}}$ and ζ_k^{mmse} is set to meet power constraint $\text{tr}((\mathbf{P}_k^{\text{mmse}})^H \mathbf{P}_k^{\text{mmse}}) = U$.

B. Asymptotic Achievable Sum-Rate

In this subsection, we investigate the asymptotic achievable sum-rate performance for the MMSE based receiver and precoder.

From the previous subsection, the UL ergodic achievable sum-rate for the MMSE receiver can be expressed as¹

$$\begin{aligned} r_{\text{mmse}}^{\text{ul}} &= \frac{1}{N_v} \sum_{k \in \mathcal{K}} \sum_{u=1}^U \mathbb{E}_{\mathbf{H}_k} \left\{ \log_2 \left\{ 1 \right. \right. \\ &\quad \left. \left. + \frac{|\mathbf{r}_{u,k}^{\text{mmse}} \mathbf{h}_{u,k}|^2 q^{\text{ul}}}{\sum_{u' \neq u} |\mathbf{r}_{u',k}^{\text{mmse}} \mathbf{h}_{u',k}|^2 q^{\text{ul}} + \sigma^{\text{ul}} \|\mathbf{r}_{u,k}^{\text{mmse}}\|^2} \right\} \right\}, \end{aligned} \quad (30)$$

where the expectation is taken with respect to the channel realizations and the MMSE receiver, $\mathbf{r}_{u,k}^{\text{mmse}}$, for UT u is the u -th row of $\mathbf{R}_k^{\text{mmse}}$. We obtain

$$\begin{aligned} r_{\text{mmse}}^{\text{ul}} &= \frac{1}{N_v} \sum_{k \in \mathcal{K}} \sum_{u=1}^U \\ &\quad \times \mathbb{E}_{\mathbf{H}_k} \left\{ \log_2 \left\{ \left[(\rho^{\text{ul}} \mathbf{G}_k + \mathbf{I}_U)^{-1} \right]_{u,u} \right\} \right\}. \end{aligned} \quad (31)$$

For the MMSE precoder, we assume that each UT can perfectly obtain the DL CSI, which can be achieved through applying the beamforming training framework [44] with low overhead. The DL ergodic achievable sum-rate is

$$\begin{aligned} r_{\text{mmse}}^{\text{dl}} &= \frac{1}{N_v} \sum_{k \in \mathcal{K}} \sum_{u=1}^U \\ &\quad \times \mathbb{E}_{\mathbf{H}_k} \left\{ \log_2 \left\{ 1 + \frac{|\mathbf{h}_{u,k}^T \mathbf{P}_{u,k}^{\text{mmse}}|^2 q^{\text{dl}}}{\sum_{u' \neq u} |\mathbf{h}_{u',k}^T \mathbf{P}_{u',k}^{\text{mmse}}|^2 q^{\text{dl}} + \sigma^{\text{dl}}} \right\} \right\}, \end{aligned} \quad (32)$$

¹The ergodic achievable sum-rate is computed by averaging along the valid subcarriers to acquire an average sum-rate performance for the wideband OFDM system.

where the MMSE precoder, $\mathbf{p}_{u,k}^{\text{mmse}}$, for UT u is the u -th column of $\mathbf{P}_k^{\text{mmse}}$. We denote $\Psi_k = (\rho^{\text{dl}} \mathbf{G}_k + \mathbf{I}_U)^{-1}$ and $\Pi_k = \left(\mathbf{G}_k + \frac{1}{\rho^{\text{dl}}} \mathbf{I}_U \right)^{-1} \mathbf{G}_k$ for notational convenience, and obtain (33), shown at the bottom of the next page.

Due to the small angle spread in HF skywave communications, we assume that channels of arbitrary two UTs have non-overlapping directional cosine sets.

Assumption 1: For arbitrary UT u and UT u' , and $u \neq u'$, we assume their directional cosine sets are non-overlapped, that is,

$$\mathcal{P}_u \cap \mathcal{P}_{u'} = \emptyset. \quad (34)$$

Under the above assumption, we have the asymptotically orthogonality of the channels between arbitrary two UTs with the channel models established in the previous section, which is expressed in Lemma 1 and proved in Appendix A.

Lemma 1: Under Assumption 1, for arbitrary $u \neq u'$, as M tends to infinity, we have

$$\lim_{M \rightarrow \infty} \frac{1}{M} \mathbf{h}_{u,k}^H \mathbf{h}_{u',k} = \sum_{p=1}^{P_u} |\varphi_{u,p}|^2, \quad (35)$$

$$\lim_{M \rightarrow \infty} \frac{1}{M} \mathbf{h}_{u,k}^H \mathbf{h}_{u',k} = 0. \quad (36)$$

Lemma 1 shows when the number of BS antennas tends to be large, the scaled channel vectors of UTs with non-overlapped directional cosine sets tend to be orthogonal. Let \tilde{P}_u denote the number of distinct non-zero elements in ω_u and $\xi_{u,1}, \dots, \xi_{u,\tilde{P}_u}$ denote the distinct non-zero elements, in decreasing order, with multiplicities $r_{u,1}, \dots, r_{u,\tilde{P}_u}$, respectively. We can obtain an UL asymptotic achievable sum-rate and its upper bound, expressed in Theorem 1 and proved in Appendix B.

Theorem 1: If the transmit power of each UT is scaled down by $1/M$ according to $q^{\text{ul}} = \epsilon^{\text{ul}}/M$ and ϵ^{ul} is fixed. Under Assumption 1, we have

$$\lim_{M \rightarrow \infty} (r_{\text{mmse}}^{\text{ul}} - \tilde{r}_{\text{mmse}}^{\text{ul}}) = 0, \quad (37)$$

where UL asymptotic achievable sum-rate $\tilde{r}_{\text{mmse}}^{\text{ul}}$ is given by (38), shown at the bottom of the next page, where $\Psi_{u,p,l}$ is defined as (39), shown at the bottom of the next page, with $\mathbf{i}_u = [i_{u,1}, \dots, i_{u,\tilde{P}_u}]^T \in \mathbb{Z}^{\tilde{P}_u \times 1}$ from the set $\mathcal{I}_{u,p,l}$ defined as (40), shown at the bottom of the next page. Moreover, $\tilde{r}_{\text{mmse}}^{\text{ul}}$ is upper bounded by

$$\tilde{r}_{\text{mmse}}^{\text{ul}} \leq \tilde{r}_{\text{mmse}}^{\text{ul,ub}} = \sum_{u=1}^U \log_2 \left\{ 1 + \frac{\epsilon^{\text{ul}}}{\sigma^{\text{ul}}} C_u \right\}, \quad (41)$$

where $C_u = \sum_{p=1}^{P_u} \sum_{q=1}^{Q_p} \beta_{u,p,q}^2$ represents the average channel power of UT u .

From Theorem 1, the UL asymptotic achievable sum-rate can be easily computed including the sum of generalized exponential integral functions, thus avoiding computational intensive expectation operation as involved in the computation of UL ergodic achievable sum-rate. Meanwhile, both UL asymptotic achievable sum-rate and its upper bound are only related to the statistical CSI. Similarly, we obtain a

DL asymptotic achievable sum-rate and its approximation, expressed in Theorem 2 and proved in Appendix C.

Theorem 2: Let $q^{\text{dl}} = \epsilon^{\text{dl}}/M$ with fixed ϵ^{dl} . Under Assumption 1, we have

$$\lim_{M \rightarrow \infty} (r_{\text{mmse}}^{\text{dl}} - \tilde{r}_{\text{mmse}}^{\text{dl}}) = 0, \quad (42)$$

where DL asymptotic achievable sum-rate $\tilde{r}_{\text{mmse}}^{\text{dl}}$ is

$$\begin{aligned} \tilde{r}_{\text{mmse}}^{\text{dl}} &= \sum_{u=1}^U \\ &\times \mathbb{E} \left\{ \log_2 \left\{ 1 + \frac{1 - \frac{2\sigma^{\text{dl}}}{\epsilon^{\text{dl}}} a_{u,1} + \left(\frac{\sigma^{\text{dl}}}{\epsilon^{\text{dl}}}\right)^2 a_{u,2}}{\frac{\sigma^{\text{dl}}}{U\epsilon^{\text{dl}}} \sum_{u=1}^U (a_{u,1} - \frac{\sigma^{\text{dl}}}{\epsilon^{\text{dl}}} a_{u,2})} \right\} \right\}, \end{aligned} \quad (43)$$

where $a_{u,1} = \left(\sum_{p=1}^{P_u} |\varphi_{u,p}|^2 + \sigma^{\text{dl}}/\epsilon^{\text{dl}}\right)^{-1}$ and $a_{u,2} = \left(\sum_{p=1}^{P_u} |\varphi_{u,p}|^2 + \sigma^{\text{dl}}/\epsilon^{\text{dl}}\right)^{-2}$. Moreover, $\tilde{r}_{\text{mmse}}^{\text{dl}}$ can be approximated by (44), shown at the bottom of the next page, where

$$b_{u,p,l,1} = (-\xi_{u,p})^{r_{u,p}-l} \Psi_{u,p,l} e^{\frac{\sigma^{\text{dl}}}{\epsilon^{\text{dl}} \xi_{u,p}}} E_{r_{u,p}-l+1} \left(\frac{\sigma^{\text{dl}}}{\epsilon^{\text{dl}} \xi_{u,p}} \right), \quad (45)$$

$$\begin{aligned} b_{u,p,l,2} &= (-\xi_{u,p})^{r_{u,p}-l-1} \Psi_{u,p,l} e^{\frac{\sigma^{\text{dl}}}{\epsilon^{\text{dl}} \xi_{u,p}}} \\ &\cdot \left(E_{r_{u,p}-l+1} \left(\frac{\sigma^{\text{dl}}}{\epsilon^{\text{dl}} \xi_{u,p}} \right) - E_{r_{u,p}-l} \left(\frac{\sigma^{\text{dl}}}{\epsilon^{\text{dl}} \xi_{u,p}} \right) \right). \end{aligned} \quad (46)$$

In Theorem 2, we provide an approximation of the DL asymptotic achievable sum-rate, which can be computed without expectation and is close to the asymptotic one, as confirmed in the simulation results. Note that the asymptotic achievable sum-rate analyses for the MMSE based receiver and precoder in terrestrial cellular communications have been

investigated in, *e.g.*, [45], [46], which are based on the independent and identically distributed (i.i.d.) channel assumption. Our results in Theorem 1 and Theorem 2 are based on the established HF skywave massive MIMO channel model with spatial correlation.

Next, we obtain the UL power-scaling law by making an insight in the UL asymptotic achievable sum-rate upper bound. The DL one can be similarly obtained and is omitted here for brevity. If we further assume equal channel power among UTs as $C_1 = \dots = C_U = C$, then $\tilde{r}_{\text{mmse}}^{\text{ul,ub}}$ can be rewritten as

$$\tilde{r}_{\text{mmse}}^{\text{ul,ub}} = U \log_2 \left\{ 1 + \frac{\epsilon^{\text{ul}}}{\sigma^{\text{ul}}} C \right\}. \quad (47)$$

Therefore, when M is sufficiently large and the UTs have non-overlapped directional cosine sets, we can scale down the transmit power per UT proportionally to $1/M$ to obtain an equal rate performance. Meanwhile, we can increase the sum-rate U times by simultaneously serving U UTs in the same time-frequency resource.

C. Low-Complexity PE Receiver and Precoder

In this subsection, we propose low-complexity PE based receiver and precoder by replacing the computationally complex matrix inversion involved in (26) and (29) with an approximate matrix polynomial and calculate the coefficients based on deterministic equivalents.

Using the Cayley-Hamilton theorem, we express the N -order PE receiver as

$$\mathbf{R}_k^{\text{pe}} = \sum_{n=1}^N b_{k,n}^{\text{ul}} \mathbf{G}_k^{n-1} \mathbf{H}_k^H, \quad (48)$$

where $N \leq U$ and $b_{k,n}^{\text{ul}}$ is the coefficient for the PE receiver. Let $\mathbf{b}_k^{\text{ul}} = [b_{k,1}^{\text{ul}}, \dots, b_{k,N}^{\text{ul}}]^T \in \mathbb{C}^{N \times 1}$ be the coefficient vector, obtained by applying the MMSE criterion

$$r_{\text{mmse}}^{\text{dl}} = \frac{1}{N_v} \sum_{k \in \mathcal{K}} \sum_{u=1}^U \mathbb{E}_{\mathbf{H}_k} \left\{ \log_2 \left\{ 1 + \frac{([\Psi_k]_{u,u} - 1) [\mathbf{\Pi}_k]_{u,u}^2}{([\mathbf{\Pi}_k \Psi_k]_{u,u} - \frac{1}{U} \text{tr}(\mathbf{\Pi}_k \Psi_k))(1 - [\Psi_k]_{u,u}) - [\Psi_k]_{u,u} [\mathbf{\Pi}_k]_{u,u}^2} \right\} \right\} \quad (33)$$

$$\tilde{r}_{\text{mmse}}^{\text{ul}} = \sum_{u=1}^U \prod_{\tilde{p}=1}^{\tilde{P}_u} \frac{1}{\xi_{u,\tilde{p}}^{r_{u,\tilde{p}}}} \sum_{p=1}^{\tilde{P}_u} \sum_{l=1}^{r_{u,p}} \frac{(-1)^{r_{u,p}-l} \Psi_{u,p,l} \xi_{u,p}^{r_{u,p}-l+1}}{\ln 2} e^{\frac{\sigma^{\text{ul}}}{\epsilon^{\text{ul}} \xi_{u,p}}} \sum_{j=0}^{r_{u,p}-l} E_{j+1} \left(\frac{\sigma^{\text{ul}}}{\epsilon^{\text{ul}} \xi_{u,p}} \right) \quad (38)$$

$$\Psi_{u,p,l} = (-1)^{r_{u,p}-1} \sum_{\mathbf{i}_u \in \mathcal{I}_{u,p,l}} \prod_{j \neq p} \frac{(i_{u,j} + r_{u,j} - 1)!}{(i_{u,j})! (r_{u,j} - 1)!} \left(\frac{1}{\xi_{u,j}} - \frac{1}{\xi_{u,p}} \right)^{-(r_{u,j} + i_{u,j})} \quad (39)$$

$$\mathcal{I}_{u,p,l} = \left\{ [i_{u,1}, \dots, i_{u,\tilde{P}_u}]^T ; \sum_{j=1}^{\tilde{P}_u} i_{u,j} = l - 1, i_{u,p} = 0, i_{u,j} \geq 0, j = 1, \dots, \tilde{P}_u \right\} \quad (40)$$

as

$$\mathbf{b}_k^{\text{ul}} = \arg \min_{\mathbf{b}_k = [b_{k,1}, \dots, b_{k,N}]^T} \mathbb{E} \left\{ \left\| \mathbf{x}_k^{\text{ul}} - \sum_{n=1}^N b_{k,n} \mathbf{G}_k^{n-1} \mathbf{H}_k^H \mathbf{y}_k^{\text{ul}} \right\|^2 \right\}. \quad (49)$$

Let $\mathbf{B}_k = \mathbf{H}_k \mathbf{H}_k^H$ and $\mu_{k,n}$ denote the n -order empirical moment $\frac{1}{M} \text{tr}(\mathbf{B}_k^n)$. Then, we have

$$\mathbf{b}_k^{\text{ul}} = (\Phi_k^{\text{ul}})^{-1} \mathbf{a}_k, \quad (50)$$

where $\Phi_k^{\text{ul}} \in \mathbb{C}^{N \times N}$ and $\mathbf{a}_k \in \mathbb{C}^{N \times 1}$ with

$$[\Phi_k^{\text{ul}}]_{i,j} = \mu_{k,i+j} + \frac{\mu_{k,i+j-1}}{\rho^{\text{ul}}}, \quad (51)$$

$$[\mathbf{a}_k]_n = \mu_{k,n}. \quad (52)$$

For the DL, the N -order PE precoder can be expressed as

$$\mathbf{P}_k^{\text{pe}} = \left(\sum_{n=1}^N b_{k,n}^{\text{dl}} \mathbf{G}_k^{n-1} \mathbf{H}_k^H \right)^T, \quad (53)$$

where $b_{k,n}^{\text{dl}}$ is the coefficient for the PE precoder. Let $\mathbf{b}_k^{\text{dl}} = [b_{k,1}^{\text{dl}}, \dots, b_{k,N}^{\text{dl}}]^T \in \mathbb{C}^{N \times 1}$ be the coefficient vector, obtained by applying the MMSE criterion as (54), shown at the bottom of the next page. Then, we have

$$\mathbf{b}_k^{\text{dl}} = \frac{1}{\zeta_k^{\text{pe}}} (\Phi_k^{\text{dl}})^{-1} \mathbf{a}_k, \quad (55)$$

where $\Phi_k^{\text{dl}} \in \mathbb{C}^{N \times N}$ with

$$[\Phi_k^{\text{dl}}]_{i,j} = \mu_{k,i+j} + \frac{\mu_{k,i+j-1}}{\rho^{\text{dl}}}, \quad (56)$$

and ζ_k^{pe} is a real scalar parameter to meet power constraint $\text{tr}((\mathbf{P}_k^{\text{pe}})^H \mathbf{P}_k^{\text{pe}}) = U$.

Note that \mathbf{b}_k^{ul} and \mathbf{b}_k^{dl} need to be computed from the empirical moments $\mu_{k,n}$ for each channel realization, which is computationally intensive. Since the statistical CSI varies very slowly with time, we compute \mathbf{b}_k^{ul} and \mathbf{b}_k^{dl} with statistical CSI. From [29, Theorem 1],

$$\lim_{M \rightarrow \infty} \mu_{k,n} - \mathbb{E}\{\mu_{k,n}\} = 0, \quad (57)$$

where the expectation is usually calculated by performing a large number of Monte-Carlo simulation, which is still computationally intensive. Next, we turn to the deterministic equivalent of $\mathbb{E}\{\mu_{k,n}\}$, denoted by $\bar{\mu}_{k,n}$, which is independent of a particular realization of \mathbf{H}_k and can be calculated based on the statistical CSI [29].

To compute $\bar{\mu}_{k,n}$, we first generate a diagonal matrix Λ_u with $\text{diag}(\Lambda_u) = \boldsymbol{\omega}_u$. Let $\Xi_{u,k}$ denote the channel correlation matrix $\mathbb{E}\{\mathbf{h}_{u,k} \mathbf{h}_{u,k}^H\}$ and we calculate

$$\Xi_{u,k} = \mathbf{V}_k \Lambda_u \mathbf{V}_k^H. \quad (58)$$

Let $\Theta \in \mathbb{C}^{M \times M}$ and $\eta_{u,k}(\Theta)$ denote $\mathbb{E}\{\mathbf{h}_{u,k}^H \Theta \mathbf{h}_{u,k}\}$. We calculate

$$\eta_{u,k}(\Theta) = \text{tr}(\mathbf{V}_k \Lambda_u \mathbf{V}_k^H \Theta). \quad (59)$$

We obtain the following relation, which is proved in Appendix D.

Theorem 3: When M tends to infinity, we have

$$\lim_{M \rightarrow \infty} \bar{\mu}_{k,n} - \mathbb{E}\{\mu_{k,n}\} = 0, \quad (60)$$

where $\bar{\mu}_{k,n} = \frac{1}{M} \text{tr}(\bar{\mathbf{B}}_{k,n})$, and $\bar{\mathbf{B}}_{k,n}$ is obtained as

$$\bar{\mathbf{B}}_{k,n+1} = \sum_{j=0}^n \left(\sum_{u=1}^U \bar{\psi}_{u,k,j} \Xi_{u,k} \right) \bar{\mathbf{B}}_{k,n-j}, \quad (61)$$

$$\bar{\psi}_{u,k,n+1} = \sum_{j=0}^n \eta_{u,k}(\bar{\mathbf{B}}_{k,j}) \bar{\psi}_{u,k,n-j}, \quad (62)$$

where $n \in \mathbb{N}$, $\bar{\mathbf{B}}_{k,0} = \mathbf{I}_M$ and $\bar{\psi}_{u,k,0} = 1$.

From Theorem 3, as M tends to infinity, $\mathbb{E}\{\mu_{k,n}\}$ tends to be equal to its deterministic equivalent $\bar{\mu}_{k,n}$. As M becomes large in HF skywave massive MIMO communications, $\mathbb{E}\{\mu_{k,n}\}$ can be approximated by $\bar{\mu}_{k,n}$. Define $\bar{\Phi}_k^{\text{ul}} \in \mathbb{C}^{N \times N}$ and $\bar{\mathbf{a}}_k \in \mathbb{C}^{N \times 1}$ with

$$[\bar{\Phi}_k^{\text{ul}}]_{i,j} = \bar{\mu}_{k,i+j} + \frac{\bar{\mu}_{k,i+j-1}}{\rho^{\text{ul}}}, \quad (63)$$

$$[\bar{\mathbf{a}}_k]_n = \bar{\mu}_{k,n}. \quad (64)$$

The approximate coefficient vector can be obtained by

$$\bar{\mathbf{b}}_k^{\text{ul}} = (\bar{\Phi}_k^{\text{ul}})^{-1} \bar{\mathbf{a}}_k. \quad (65)$$

We denote $[\bar{\mathbf{b}}_k^{\text{ul}}]_n$ as $\bar{b}_{k,n}^{\text{ul}}$, and the low-complexity PE receiver can be expressed as

$$\bar{\mathbf{R}}_k^{\text{pe}} = \sum_{n=1}^N \bar{b}_{k,n}^{\text{ul}} \mathbf{G}_k^{n-1} \mathbf{H}_k^H. \quad (66)$$

The UL ergodic achievable sum-rate for the low-complexity PE receiver, $\bar{\mathbf{R}}_k^{\text{pe}}$, is given by

$$r_{\text{pe}}^{\text{ul}} = \frac{1}{N_v} \sum_{k \in \mathcal{K}} \sum_{u=1}^U \mathbb{E}_{\mathbf{H}_k} \left\{ \log_2 \left\{ 1 + \frac{|\bar{\mathbf{r}}_{u,k}^{\text{pe}} \mathbf{h}_{u,k}|^2 q^{\text{ul}}}{\sum_{u' \neq u} |\bar{\mathbf{r}}_{u',k}^{\text{pe}} \mathbf{h}_{u',k}|^2 q^{\text{ul}} + \sigma^{\text{ul}} \|\bar{\mathbf{r}}_{u,k}^{\text{pe}}\|^2} \right\} \right\}, \quad (67)$$

$$\tilde{r}_{\text{mmse}}^{\text{dl}} \approx \tilde{r}_{\text{mmse}}^{\text{dl,appro}} = \sum_{u=1}^U \log_2 \left\{ 1 + \frac{1 - \prod_{\tilde{p}=1}^{\tilde{P}_u} \frac{1}{\xi_{u,\tilde{p}}^{r_{u,p}}} \sum_{p=1}^{\tilde{P}_u} \sum_{l=1}^{r_{u,p}} \left(\frac{2\sigma_{\epsilon}^{\text{dl}}}{\epsilon^{\text{dl}}} b_{u,p,l,1} - \left(\frac{\sigma_{\epsilon}^{\text{dl}}}{\epsilon^{\text{dl}}} \right)^2 b_{u,p,l,2} \right)}{\prod_{u=1}^U \frac{\sigma_{\epsilon}^{\text{dl}}}{\epsilon^{\text{dl}}} \sum_{u=1}^U \prod_{\tilde{p}=1}^{\tilde{P}_u} \frac{1}{\xi_{u,\tilde{p}}^{r_{u,p}}} \sum_{p=1}^{\tilde{P}_u} \sum_{l=1}^{r_{u,p}} \left(b_{u,p,l,1} - \frac{\sigma_{\epsilon}^{\text{dl}}}{\epsilon^{\text{dl}}} b_{u,p,l,2} \right)} \right\} \quad (44)$$

where the low-complexity PE receiver, $\bar{\mathbf{r}}_{u,k}^{\text{pe}}$, for UT u is the u -th row of $\bar{\mathbf{R}}_k^{\text{pe}}$.

Similarly, the low-complexity PE precoder can be expressed as

$$\bar{\mathbf{P}}_k^{\text{pe}} = \left(\sum_{n=1}^N \bar{b}_{k,n}^{\text{dl}} \mathbf{G}_k^{n-1} \mathbf{H}_k^H \right)^T, \quad (68)$$

where $\bar{b}_{k,n}^{\text{dl}}$ is the approximate coefficient. We denote $\bar{\mathbf{b}}_k^{\text{dl}} = [\bar{b}_{k,1}^{\text{dl}}, \dots, \bar{b}_{k,N}^{\text{dl}}]^T \in \mathbb{C}^{N \times 1}$, obtained as

$$\bar{\mathbf{b}}_k^{\text{dl}} = \frac{1}{\zeta_k^{\text{pe}}} (\bar{\Phi}_k^{\text{dl}})^{-1} \bar{\mathbf{a}}_k, \quad (69)$$

where $\bar{\Phi}_k^{\text{dl}} \in \mathbb{C}^{N \times N}$ with

$$[\bar{\Phi}_k^{\text{dl}}]_{i,j} = \bar{\mu}_{k,i+j} + \frac{\bar{\mu}_{k,i+j-1}}{\rho^{\text{dl}}}, \quad (70)$$

and ζ_k^{pe} is a real scalar parameter to meet power constraint $\text{tr} \left(\left(\bar{\mathbf{P}}_k^{\text{pe}} \right)^H \bar{\mathbf{P}}_k^{\text{pe}} \right) = U$. The DL ergodic achievable sum-rate for the low-complexity PE precoder, $\bar{\mathbf{P}}_k^{\text{pe}}$, is given by

$$r_{\text{pe}}^{\text{dl}} = \frac{1}{N_v} \sum_{k \in \mathcal{K}} \sum_{u=1}^U \mathbb{E}_{\mathbf{H}_k} \left\{ \log_2 \left\{ 1 + \frac{|\mathbf{h}_{u,k}^T \bar{\mathbf{P}}_{u,k}^{\text{pe}}|^2 q^{\text{dl}}}{\sum_{u' \neq u} |\mathbf{h}_{u,k}^T \bar{\mathbf{P}}_{u',k}^{\text{pe}}|^2 q^{\text{dl}} + \sigma^{\text{dl}}} \right\} \right\}, \quad (71)$$

where the low-complexity PE precoder, $\bar{\mathbf{P}}_{u,k}^{\text{pe}}$, for UT u is the u -th column of $\bar{\mathbf{P}}_k^{\text{pe}}$.

We compare the computational complexity of the MMSE and low-complexity PE receivers in terms of complex multiplications required, while the DL result can be similarly obtained and is omitted for brevity. For the PE receiver, the complexity of computing $\bar{\mathbf{b}}_k^{\text{ul}}$ is dominated by the computation of $\bar{\mu}_{k,n}$, which is of order $\mathcal{O}(U^3)$ and the computation process needs to be performed only when the slow-varying statistical CSI change [29]. For given $\bar{\mathbf{b}}_k^{\text{ul}}$, the low-complexity advantage of the PE receiver has been confirmed in [29], [47]. By exploiting Horner's scheme [48], $\bar{\mathbf{R}}_k^{\text{pe}}$ needs not to be explicitly computed and no matrix-matrix multiplications are involved to obtain $\bar{\mathbf{R}}_k^{\text{pe}} \mathbf{y}_k^{\text{ul}}$, *i.e.*,

$$\bar{\mathbf{R}}_k^{\text{pe}} \mathbf{y}_k^{\text{ul}} = b_{k,1}^{\text{ul}} \tilde{\mathbf{y}}_k^{\text{ul}} + b_{k,2}^{\text{ul}} \tilde{\mathbf{H}}_k^H \mathbf{H}_k \cdot \left(\tilde{\mathbf{y}}_k^{\text{ul}} + (b_{k,3}^{\text{ul}}/b_{k,2}^{\text{ul}}) \tilde{\mathbf{H}}_k^H \mathbf{H}_k (\tilde{\mathbf{y}}_k^{\text{ul}} + \dots) \right), \quad (72)$$

where $\tilde{\mathbf{y}}_k^{\text{ul}} = \tilde{\mathbf{H}}_k^H \mathbf{y}_k^{\text{ul}}$ and the overall computational complexity is $(2N - 1)MU$. For the MMSE receiver, the design complexity of $\mathbf{R}_k^{\text{mmse}}$ is $0.5MU(U + 1) + 0.5U^3 + 1.5U^2 + MU^2$ [49], and the computational complexity is MU to obtain $\mathbf{R}_k^{\text{mmse}} \mathbf{y}_k^{\text{ul}}$. The total computational complexity of the PE receiver can be much lower than that of the MMSE receiver although the computational complexity of (72) is larger than that of $\mathbf{R}_k^{\text{mmse}} \mathbf{y}_k^{\text{ul}}$ when $N > 1$.

In order to reduce the computational complexity of $\bar{\mathbf{R}}_k^{\text{pe}} \mathbf{y}_k^{\text{ul}}$, the specific structure of the HF skywave channel represented by the proposed beam based channel model in (21) can be exploited. We rewrite (72) as

$$\bar{\mathbf{R}}_k^{\text{pe}} \mathbf{y}_k^{\text{ul}} = b_{k,1}^{\text{ul}} \tilde{\mathbf{y}}_k^{\text{ul}} + b_{k,2}^{\text{ul}} \tilde{\mathbf{H}}_k^H \mathbf{V}_k^H \mathbf{V}_k \tilde{\mathbf{H}}_k \cdot \left(\tilde{\mathbf{y}}_k^{\text{ul}} + (b_{k,3}^{\text{ul}}/b_{k,2}^{\text{ul}}) \tilde{\mathbf{H}}_k^H \mathbf{V}_k^H \mathbf{V}_k \tilde{\mathbf{H}}_k (\tilde{\mathbf{y}}_k^{\text{ul}} + \dots) \right), \quad (73)$$

where $\tilde{\mathbf{y}}_k^{\text{ul}} = \tilde{\mathbf{H}}_k^H \mathbf{V}_k^H \mathbf{y}_k^{\text{ul}}$ and $\tilde{\mathbf{H}}_k = [\tilde{\mathbf{h}}_{1,k}, \dots, \tilde{\mathbf{h}}_{U,k}] \in \mathbb{C}^{\tilde{M} \times U}$ denote the beam domain channel matrix. We note that the multiplication of \mathbf{V}_k^H (or \mathbf{V}_k) and a given $M \times 1$ (or $\tilde{M} \times 1$) vector can be efficiently computed by applying chirp zeta transform [50]. The complexity is $M + L + \tilde{M} + L \log_2 L$, where $L \geq M + \tilde{M} - 1$. The multiplication of $\tilde{\mathbf{H}}_k^H$ (or $\tilde{\mathbf{H}}_k$) and a given $\tilde{M} \times 1$ (or $U \times 1$) vector can be efficiently computed by exploiting the sparsity property of $\tilde{\mathbf{H}}_k$, thanks to the small angle spread of the HF skywave massive MIMO channels. Denote the number of non-zero elements in ω_u as \tilde{M}_u for $u = 1, \dots, U$. Let \tilde{M}^{ave} be the average value of $\tilde{M}_1, \dots, \tilde{M}_U$, *i.e.*, $\tilde{M}^{\text{ave}} = \sum_{u=1}^U \tilde{M}_u / U$, and obviously $\tilde{M}^{\text{ave}} \ll \tilde{M}$. For example, in the simulation, we obtain $\tilde{M}^{\text{ave}} = 3.16$, while \tilde{M} is 512. Then, the complexity of the multiplication of $\tilde{\mathbf{H}}_k^H$ (or $\tilde{\mathbf{H}}_k$) and a given $\tilde{M} \times 1$ (or $U \times 1$) vector is $U \tilde{M}^{\text{ave}}$. In summary, the overall complexity of (73) is $(2N - 1) (M + L + \tilde{M} + L \log_2 L + U \tilde{M}^{\text{ave}})$. Compared with (72), the complexity advantage of (73) will be obvious when both M and U become large.

IV. SIMULATION RESULTS

In this section, we provide simulation results to show the performance of the proposed HF skywave massive MIMO communications.

A. Ray-Tracing Channels and Noise Power

In the simulation, we consider a wideband HF skywave massive MIMO-OFDM system and the major parameters are summarized in Table I. The latitude and longitude of the BS are set as 34°N and 118°E , respectively. Totally, 500 UTs are

$$\mathbf{b}_k^{\text{dl}} = \arg \min_{\mathbf{b}_k} \mathbb{E} \left\{ \left\| \mathbf{x}_k^{\text{dl}} - \zeta_k \mathbf{H}_k^T \left(\sum_{n=1}^N b_{k,n} \mathbf{G}_k^{n-1} \mathbf{H}_k^H \right)^T \mathbf{x}_k^{\text{dl}} - \zeta_k \mathbf{z}_k^{\text{dl}} \right\|^2 \right\} \\ \text{s.t. } \text{tr} \left(\left(\sum_{n=1}^N b_{k,n} \mathbf{G}_k^{n-1} \mathbf{H}_k^H \right)^* \left(\sum_{n=1}^N b_{k,n} \mathbf{G}_k^{n-1} \mathbf{H}_k^H \right)^T \right) \leq U \quad (54)$$

TABLE I
HF SKYWAVE MASSIVE MIMO-OFDM SYSTEM PARAMETERS

Parameter	Value
Carrier frequency f_c	16 MHz
BS antenna spacing d	9 m
System bandwidth B	384 kHz
Sampling interval T_s	1.95 μ s
Subcarrier spacing Δf	250 Hz
Subcarrier number N_c	2048
CP length N_g	512

generated and the great circle distances between the BS and the UTs are set equally as 2,000 km. The azimuth angles of the UTs seen from the BS are randomly generated in the interval $(-90^\circ, 90^\circ)$, then we can find the UT's latitude and longitude by solving the direct geodetic problem [51].

To obtain a realistic HF skywave channel, we generate the channel parameters with the aid of a commercial ray-tracing software, Proplab-Pro version 3.1 [52]. The 3D ray-tracing technique used by the software is the Appleton-Hartree type and takes into consideration both the magnetic field's influence and the collision effect. The dipole field model is selected for the magnetic field with two exponential terms as the collision frequency model.

We select the time for ray tracing at 11:00 coordinated universal time on March 10, 2021. Then, we perform the ray-tracing process for a given BS-UT link, where isotropic antennas are assumed for both ends. Ray launching is performed by emitting rays from the BS into all directions. The effective paths are identified as emerging at a given distance of the UT. For each extracted effective path, the ray-tracing results are signal strength, propagation distance, azimuth AoD, and elevation AoD. We can obtain the average path gain and propagation delay accordingly. Using the ray-tracing generated path parameters and randomly generated initial phases and Doppler shifts for subpaths, we generate the channel vector and statistical CSI according to (15) and (23), respectively.

The noise power σ in dBW available at the terminals of a lossless antenna is given by [53]

$$\sigma = 10 \log_{10} B + F - 204, \quad (74)$$

where B is the system bandwidth and F is the antenna noise power factor, which is related to the position of the BS and UTs [53]. For simplicity, the noise powers at the UTs are set equally and are the same with that at the BS. In the following, we set the noise power in an one Hz bandwidth as $F - 204 = -163$ dBW at the BS and UTs according to voice of America coverage analysis program (VOACAP), which is a well-known ionospheric propagation prediction program [54].

B. Achievable Sum-Rate Performance

Based on the ray-tracing channels, we perform achievable sum-rate simulation for the proposed transmission strategies. We define the correlation between UT u and u' as

$$\gamma_{u,u'} = \frac{1}{N_v} \sum_{k \in \mathcal{K}} \frac{\text{tr}(\mathbf{\Xi}_{u,k} \mathbf{\Xi}_{u',k})}{\|\mathbf{\Xi}_{u,k}\|_F \|\mathbf{\Xi}_{u',k}\|_F}. \quad (75)$$

In each of the following simulation instances, we perform the user scheduling process to select UTs with sufficiently low correlation following a similar method provided in [55, Algorithm 1]. We obtain the simulated sum-rate, asymptotic sum-rate, and its upper bound for the MMSE receiver based on (31), (38), and (41), respectively. We also obtain the simulated sum-rate, asymptotic sum-rate, and its approximation for the MMSE precoder based on (33), (43), and (44), respectively.

In Fig. 2, we evaluate the sum-rate performance for the MMSE based receiver and precoder versus the total transmit power, where the total transmit power refers to the sum of the transmit powers of the UTs for a system bandwidth of 384 kHz. We set $M = 256$, $\bar{M} = 512$, and $U = 64$. From the figure, for the UL, the simulated sum-rate is close to the asymptotic one due to the limited inter-user interference and the asymptotic sum-rate upper bound is tight, especially at a low transmit power level. For the DL, the gap between the simulated sum-rate and the asymptotic one is larger than that of the UL case and the asymptotic sum-rate approximation is almost the same as the asymptotic one. Meanwhile, as the total transmit power increases, the gap between the simulated sum-rates and the asymptotic ones increases. The reason lies in the fact that in the high total transmit power region, the impact of inter-UT interference becomes obvious. Moreover, the inter-UT interference vanishes for the asymptotic sum-rates, despite the total transmit power. In addition, the sum-rates for the MMSE based receiver and precoder grow nearly linearly with the total transmit power (in dBW) when it is larger than 20 dBW.

In Fig. 3, we evaluate the sum-rate performance for the MMSE based receiver and precoder versus the number of BS antennas at fixed $q^{\text{ul}} = q^{\text{dl}} = 5$ dBW, $q^{\text{ul}} = \epsilon^{\text{ul}}/M$, and $q^{\text{dl}} = \epsilon^{\text{dl}}/M$ with $\epsilon^{\text{ul}} = \epsilon^{\text{dl}} = 30$ dBW. We set $U = 64$ and $\bar{M} = 2M$. From the figure, the UL/DL simulated sum-rates are close to the asymptotic ones, especially when M is large, which means that the inter-user interference can be small. When M is small, the gaps between the simulated sum-rates and the asymptotic ones become obvious due to serious inter-user interference caused by the poor resolution of a small antenna array. In addition, for fixed q^{ul} and q^{dl} , the sum-rates grow without a bound (logarithmically fast with M) when M grows large. If $q^{\text{ul}} = \epsilon^{\text{ul}}/M$ and $q^{\text{dl}} = \epsilon^{\text{dl}}/M$, the sum-rates approach a constant value as M increases, which confirms that we can scale down the transmit power proportionally to $1/M$ for large M .

In Fig. 4, we evaluate the sum-rate performance for the MMSE based receiver and precoder versus the number of UTs. We set $M = 256$ and $\bar{M} = 512$. The transmit power per UT is set as $q^{\text{ul}} = q^{\text{dl}} = 10$ dBW. From the figure, the sum-rates first increase almost linearly with U when U is small, and the simulated sum-rates are close to the asymptotic ones, which implies that the inter-user interferences for both the UL and DL cases are small. Furthermore, as the number of UTs increases, the gap between the simulated sum-rates and the asymptotic ones also increases. The reason lies in that the inter-UT interference may become larger with more UTs, which will affect the simulated sum-rate. Meanwhile, inter-UT interference is not involved in the asymptotic sum-rates, and

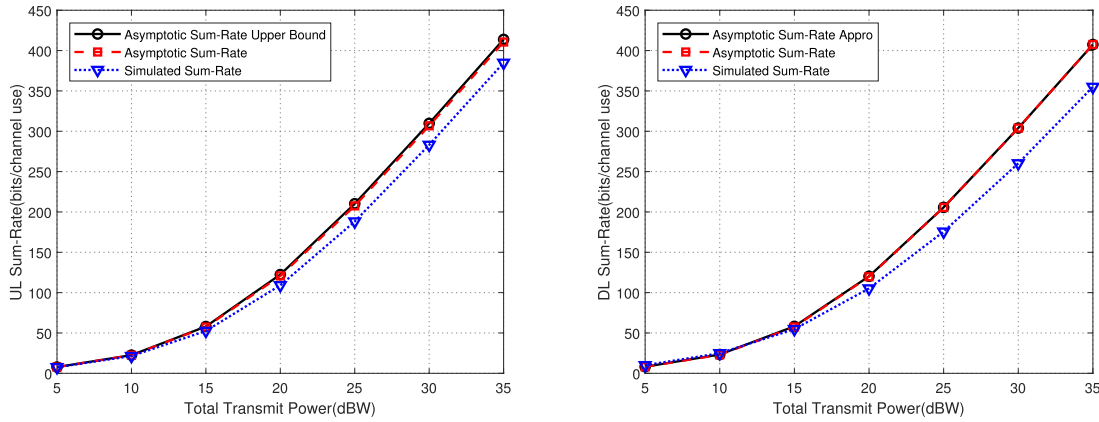


Fig. 2. Sum-rates versus the total transmit power for the MMSE based receiver and precoder.

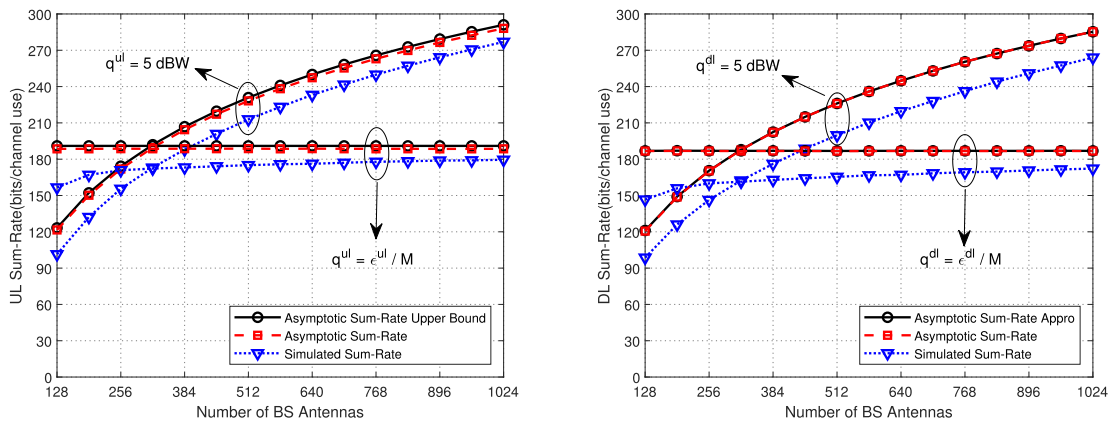


Fig. 3. Sum-rates versus the number of BS antennas for the MMSE based receiver and precoder.

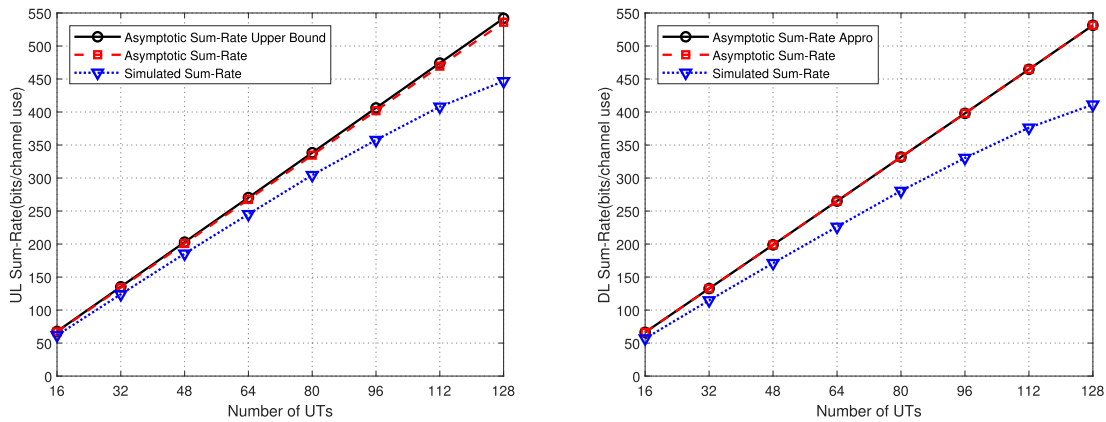


Fig. 4. Sum-rates versus the number of UTs for the MMSE based receiver and precoder.

the increase trend of the asymptotic sum-rates is almost linear with the number of UTs.

Fig. 5 compares the simulated sum-rate performance for the MMSE, ZF, PE, and low-complexity PE based receivers and precoders. We set $M = 256$, $\bar{M} = 512$, and $U = 96$. Note that when the order of PE receiver and precoder is $N = 1$, they are actually the MRC receiver and precoder, respectively. From the figure, the sum-rates for the

low-complexity PE receiver/precoder can be very close to those of the PE receiver/precoder. The ZF receiver outperforms the MRC receiver at the high total transmit power region since it maximizes the received signal-to-interference ratio. The MMSE receiver is able to achieve a better performance than the ZF receiver when the total transmit power is small. As the order N increases, the gap between the sum-rates of the low-complexity PE receiver/precoder and that of the

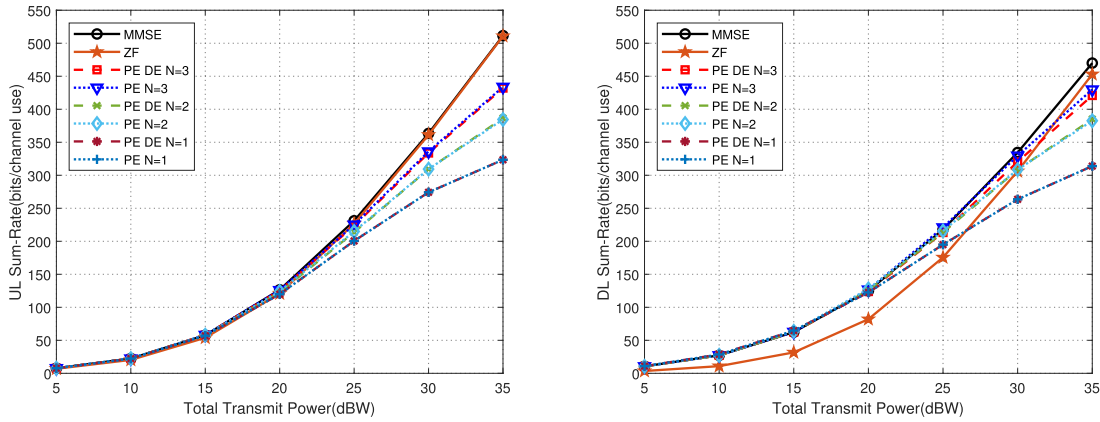


Fig. 5. Simulated sum-rates for the MMSE, ZF, PE, and low-complexity PE based receivers and precoders.

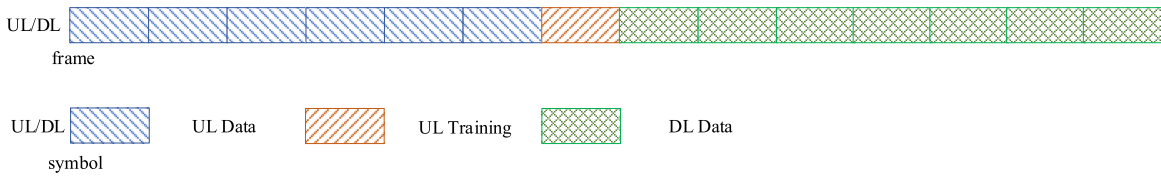


Fig. 6. TDD frame structure.

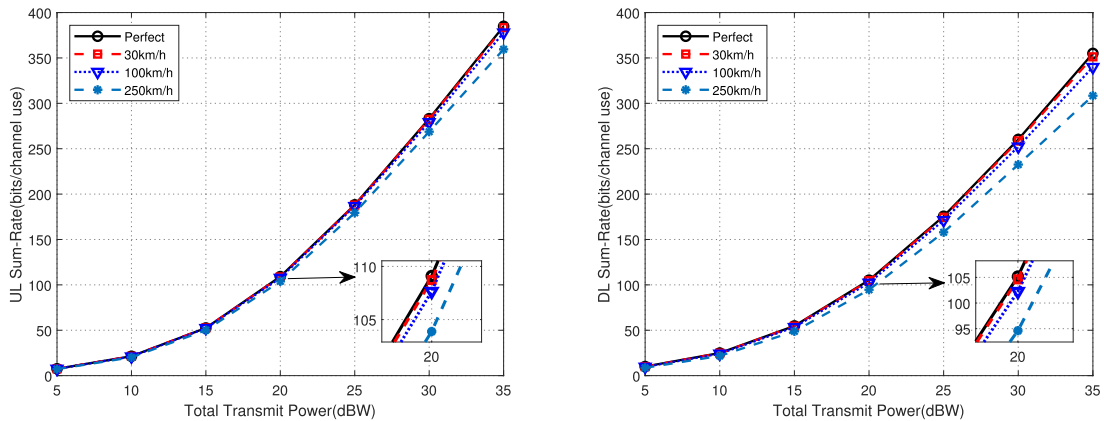


Fig. 7. Simulated sum-rates for the MMSE based receiver and precoder with different speeds of the UTs.

MMSE receiver/precoder decreases. When $N = 3$, the low-complexity PE receiver/precoder can achieve considerable sum-rate performance with the MMSE receiver/precoder but with relative low complexity.

To obtain a more realistic performance for the MMSE based UL receiver and DL precoder, we consider a TDD frame structure as shown in Fig. 6. Each frame contains 14 OFDM symbols where the UL and DL transmission each contains 7 OFDM symbols. The UL training symbol is placed between the UL data symbols and DL data symbols. One OFDM symbol is generally not enough for channel estimation of a number of UTs, when conventional orthogonal pilots are used. We can consider pilot reuse for the CSI acquisition with significantly reduced overhead [55]. The duration of one OFDM symbol is 4.99 ms according to the system parameters provided in Table I. Note that the frame structure illustrated

in Fig. 6 is an example under the configurations in the simulation and can be adaptively adjusted according to the ionospheric conditions in practice. We obtain the receiver and precoder by using the channels on the training OFDM symbol. We use the channels on the first 6 symbols to calculate the UL sum-rate for the MMSE receiver and channels on the last 7 symbols to calculate the DL sum-rate for the MMSE precoder.

In Fig. 7, we evaluate the simulated sum-rate performance for the MMSE based receiver and precoder under the TDD frame structure in Fig. 6. We set $M = 256$, $\bar{M} = 512$, and $U = 64$. The ionosphere imposed maximum Doppler spread is set to 0.5 Hz for moderate ionospheric conditions at mid-latitude regions [31]. The speeds of the UTs are set equally to 30, 100, and 250 km/h, respectively. We take the DL propagation delay into consideration while calculating the DL

sum-rate. We observe that the mobility of UTs can decrease the UL/DL sum-rates. However, the sum-rate performance loss is slight even in the case with 250 km/h due to the relatively short symbol length and long wavelength. This confirms the effectiveness of the MMSE based receiver and precoder for HF skywave massive MIMO communications.

V. CONCLUSION

In this paper, we have investigated HF skywave massive MIMO communications to achieve a significant increase in system sum-rate performance. We have presented a wideband massive MIMO-OFDM channel model for HF skywave communications. Specifically, we have derived a wideband beam based channel model and revealed that statistical CSI in the beam domain is independent of subcarriers while the beam based channel expression is different for different subcarriers for wideband transmission. We have developed the MMSE based UL receiver and DL precoder, and derived the asymptotic achievable sum-rate. The results show that for a large number of antennas M at the BS, the sum-rate can be asymptotically increased proportionally to the number of UTs while the transmit power per UT is scaled down proportionally to $1/M$. We have also proposed low-complexity PE based design for the MMSE receiver/precoder based on deterministic equivalents. We have simulated the channel with the aid of a commercial ray-tracing software, Proplab-Pro version 3.1. Based on our simulation results, massive MIMO can significantly improve the performance of HF skywave communications.

APPENDIX A PROOF OF LEMMA 1

With (18), we first calculate $\frac{1}{M}\mathbf{h}_{u,k}^H\mathbf{h}_{u,k}$ as

$$\begin{aligned} \frac{1}{M}\mathbf{h}_{u,k}^H\mathbf{h}_{u,k} &= \frac{1}{M}\sum_{\tilde{m}=1}^{\tilde{M}}\sum_{\tilde{s}\neq\tilde{m}}^{\tilde{M}}\tilde{h}_{u,k,\tilde{m}}^*\tilde{h}_{u,k,\tilde{s}}[\mathbf{v}(\gamma_{\tilde{m}},k)]^H\mathbf{v}(\gamma_{\tilde{s}},k) \\ &\quad + \sum_{\tilde{m}=1}^{\tilde{M}}\left|\tilde{h}_{u,k,\tilde{m}}\right|^2. \end{aligned} \quad (76)$$

Note that the number of channels' multipath P_u for UT u is limited. Thus, $\mathbf{h}_{u,k}$ have P_u non-zero elements as \tilde{M} tends to infinity, denoted by

$$\lim_{M\rightarrow\infty}\tilde{h}_{u,k,\tilde{m}}\rightarrow 0, \quad \text{for } \tilde{m}\neq(\Omega_{u,p}+1)\tilde{M}/2. \quad (77)$$

As M tends to infinity, we obtain

$$\sum_{\tilde{m}=1}^{\tilde{M}}\left|\tilde{h}_{u,k,\tilde{m}}\right|^2\rightarrow\sum_{p=1}^{P_u}|\varphi_{u,p}|^2, \quad \text{as } M\rightarrow\infty. \quad (78)$$

Besides, we can obtain

$$\begin{aligned} &\frac{1}{M}\left|[\mathbf{v}(\gamma_{\tilde{m}},k)]^H\mathbf{v}(\gamma_{\tilde{s}},k)\right| \\ &= \frac{1}{M}\left|\frac{\sin(2\pi(f_c+k\Delta f)\Delta\tau(\tilde{m}-\tilde{s})M/\tilde{M})}{\sin(2\pi(f_c+k\Delta f)\Delta\tau(\tilde{m}-\tilde{s})/\tilde{M})}\right|\rightarrow 0, \\ &\text{as } M\rightarrow\infty, \end{aligned} \quad (79)$$

by using simple results on geometric series. Thus, we can obtain

$$\lim_{M\rightarrow\infty}\frac{1}{M}\mathbf{h}_{u,k}^H\mathbf{h}_{u,k}=\sum_{p=1}^{P_u}|\varphi_{u,p}|^2. \quad (80)$$

Similarly, we can obtain (36). This completes the proof.

APPENDIX B PROOF OF THEOREM 1

From Lemma 1, we can express

$$\left[(\rho^{\text{ul}}\mathbf{G}_k+\mathbf{I}_U)^{-1}\right]_{u,u}\rightarrow\left(1+\frac{\epsilon^{\text{ul}}}{\sigma^{\text{ul}}}\sum_{p=1}^{P_u}|\varphi_{u,p}|^2\right)^{-1}, \quad \text{as } M\rightarrow\infty. \quad (81)$$

Thus, as M tends to infinity, we obtain

$$r_{\text{mmse}}^{\text{ul}}\rightarrow\sum_{u=1}^U\mathbb{E}\left\{\log_2\left\{1+\frac{\epsilon^{\text{ul}}}{\sigma^{\text{ul}}}\sum_{p=1}^{P_u}|\varphi_{u,p}|^2\right\}\right\}=\tilde{r}_{\text{mmse}}^{\text{ul}}, \quad \text{as } M\rightarrow\infty. \quad (82)$$

Let x_1, \dots, x_{P_u} be i.i.d. exponential random variables with unit mean and unit variance. Then, for the asymptotic case, we define $|\varphi_{u,p}|^2 = [\boldsymbol{\omega}_u]_{\tilde{m}_p} x_p$ as an exponential distributed variable where $\tilde{m}_p = (\Omega_{u,p} + 1)\tilde{M}/2$. The probability density function of $x_u = \sum_{p=1}^{P_u} [\boldsymbol{\omega}_u]_{\tilde{m}_p} x_p$ is obtained as [56]

$$f(x_u) = \prod_{\tilde{p}=1}^{\tilde{P}_u} \frac{1}{\xi_{u,\tilde{p}}} \sum_{p=1}^{\tilde{P}_u} \sum_{l=1}^{r_{u,p}} \frac{\Psi_{u,p,l}}{(r_{u,p}-l)!} (-x_u)^{r_{u,p}-l} e^{-\frac{x_u}{\xi_{u,p}}}, \quad (83)$$

where $\Psi_{u,p,l}$ is defined in (39). Then, we can calculate $\tilde{r}_{\text{mmse}}^{\text{ul}}$ in close-form as

$$\tilde{r}_{\text{mmse}}^{\text{ul}} = \sum_{u=1}^U \int_0^\infty \log_2\left\{1 + \frac{\epsilon^{\text{ul}}}{\sigma^{\text{ul}}}x_u\right\} f(x_u) dx_u, \quad (84)$$

which further leads to (38) by using the following integral formula [57]

$$\int_0^\infty \log_2(1+\gamma x)x^b e^{-\frac{x}{a}} dx = \frac{a^{b+1}}{\ln 2} b! e^{\frac{1}{\gamma a}} \sum_{j=0}^b E_{j+1}\left(\frac{1}{\gamma a}\right). \quad (85)$$

Note that function $f(x) = \log_2(1+x)$ is convex for $x > 0$. By using Jensen's inequality, $\tilde{r}_{\text{mmse}}^{\text{ul}}$ is upper bounded by

$$\begin{aligned} \tilde{r}_{\text{mmse}}^{\text{ul}} &\leq \frac{1}{N_v} \sum_{k=1}^{N_v} \sum_{u=1}^U \log_2\left\{1 + \frac{\epsilon^{\text{ul}}}{\sigma^{\text{ul}}}\mathbb{E}\left\{\sum_{p=1}^{P_u}|\varphi_{u,p}|^2\right\}\right\} \\ &\stackrel{(a)}{=} \frac{1}{N_v} \sum_{k=1}^{N_v} \sum_{u=1}^U \log_2\left\{1 + \frac{\epsilon^{\text{ul}}}{\sigma^{\text{ul}}}\sum_{p=1}^{P_u}\sum_{q=1}^{Q_p}\beta_{u,p,q}^2\right\} \\ &= \tilde{r}_{\text{mmse}}^{\text{ul,ub}}, \end{aligned} \quad (86)$$

where (a) follows from (23). This completes the proof.

APPENDIX C
PROOF OF THEOREM 2

From Lemma 1, Ψ_k and Π_k in (33) tend to be diagonal when M tends to infinity. We can express

$$[\Psi_k]_{u,u} \rightarrow \left(1 + \frac{\epsilon^{\text{dl}}}{\sigma^{\text{dl}}} \sum_{p=1}^{P_u} |\varphi_{u,p}|^2\right)^{-1}, \text{ as } M \rightarrow \infty, \quad (87)$$

$$[\Pi_k]_{u,u} \rightarrow \frac{\epsilon^{\text{dl}}}{\sigma^{\text{dl}}} \sum_{p=1}^{P_u} |\varphi_{u,p}|^2 \left(1 + \frac{\epsilon^{\text{dl}}}{\sigma^{\text{dl}}} \sum_{p=1}^{P_u} |\varphi_{u,p}|^2\right)^{-1}, \text{ as } M \rightarrow \infty. \quad (88)$$

Thus, as M tends to infinity, we obtain DL asymptotic achievable sum-rate $\tilde{r}_{\text{mmse}}^{\text{dl}}$ in (43). According to [58, Lemma 1], we obtain an approximation of $\tilde{r}_{\text{mmse}}^{\text{dl}}$ as

$$\begin{aligned} \tilde{r}_{\text{mmse}}^{\text{dl}} &\approx \frac{1}{N_v} \sum_{k \in \mathcal{K}} \sum_{u=1}^U \log_2 \left\{ 1 + \frac{1 - \frac{2\sigma^{\text{dl}}}{\epsilon^{\text{dl}}} \bar{a}_{u,1} + \left(\frac{\sigma^{\text{dl}}}{\epsilon^{\text{dl}}}\right)^2 \bar{a}_{u,2}}{\frac{\sigma^{\text{dl}}}{U \epsilon^{\text{dl}}} \sum_{u=1}^U \left(\bar{a}_{u,1} - \frac{\sigma^{\text{dl}}}{\epsilon^{\text{dl}}} \bar{a}_{u,2}\right)} \right\} \\ &= \tilde{r}_{\text{mmse}}^{\text{dl,appro}}, \end{aligned} \quad (89)$$

where $\bar{a}_{u,1} = \mathbb{E} \left\{ \left(\sum_{p=1}^{P_u} |\varphi_{u,p}|^2 + \frac{\sigma^{\text{dl}}}{\epsilon^{\text{dl}}} \right)^{-1} \right\}$ and $\bar{a}_{u,2} = \mathbb{E} \left\{ \left(\sum_{p=1}^{P_u} |\varphi_{u,p}|^2 + \frac{\sigma^{\text{dl}}}{\epsilon^{\text{dl}}} \right)^{-2} \right\}$. With the probability density function defined in (83), we can calculate

$$\bar{a}_{u,1} = \prod_{\tilde{p}=1}^{\tilde{P}_u} \frac{1}{\xi_{u,\tilde{p}}^{r_{u,\tilde{p}}}} \sum_{p=1}^{\tilde{P}_u} \sum_{l=1}^{r_{u,p}} \frac{(-1)^{r_{u,p}-l} \Psi_{u,p,l}}{(r_{u,p}-l)!} \int_0^\infty \left(x_u + \frac{\sigma^{\text{dl}}}{\epsilon^{\text{dl}}}\right)^{-1} \times x_u^{r_{u,p}-l} e^{-\frac{x_u}{\xi_{u,p}}} dx_u, \quad (90)$$

where

$$\begin{aligned} &\int_0^\infty \left(x_u + \frac{\sigma^{\text{dl}}}{\epsilon^{\text{dl}}}\right)^{-1} x_u^{r_{u,p}-l} e^{-\frac{x_u}{\xi_{u,p}}} dx_u \\ &= \ln 2 \int_0^\infty \log_2 \left\{ 1 + \frac{\epsilon^{\text{dl}}}{\sigma^{\text{dl}}} x_u \right\} \left(\frac{1}{\xi_{u,p}} x_u^{r_{u,p}-l} e^{-\frac{x_u}{\xi_{u,p}}} - (r_{u,p}-l) x_u^{r_{u,p}-l-1} e^{-\frac{x_u}{\xi_{u,p}}} \right) dx_u \\ &\stackrel{(a)}{=} \xi_{u,p}^{r_{u,p}-l} (r_{u,p}-l)! e^{\frac{\sigma^{\text{dl}}}{\epsilon^{\text{dl}} \xi_{u,p}}} E_{r_{u,p}-l+1} \left(\frac{\sigma^{\text{dl}}}{\epsilon^{\text{dl}} \xi_{u,p}} \right), \end{aligned} \quad (91)$$

and (a) follows from applying integral formula (85). Besides, we can calculate

$$\begin{aligned} \bar{a}_{u,2} &= \prod_{\tilde{p}=1}^{\tilde{P}_u} \frac{1}{\xi_{u,\tilde{p}}^{r_{u,\tilde{p}}}} \sum_{p=1}^{\tilde{P}_u} \sum_{l=1}^{r_{u,p}} \frac{(-1)^{r_{u,p}-l} \Psi_{u,p,l}}{(r_{u,p}-l)!} \\ &\quad \times \int_0^\infty \left(x_u + \frac{\sigma^{\text{dl}}}{\epsilon^{\text{dl}}}\right)^{-2} x_u^{r_{u,p}-l} e^{-\frac{x_u}{\xi_{u,p}}} dx_u, \end{aligned} \quad (92)$$

where

$$\begin{aligned} &\int_0^\infty \left(x_u + \frac{\sigma^{\text{dl}}}{\epsilon^{\text{dl}}}\right)^{-2} x_u^{r_{u,p}-l} e^{-\frac{x_u}{\xi_{u,p}}} dx_u \\ &= \int_0^\infty \left(x_u + \frac{\sigma^{\text{dl}}}{\epsilon^{\text{dl}}}\right)^{-1} \left((r_{u,p}-l) x_u^{r_{u,p}-l-1} e^{-\frac{x_u}{\xi_{u,p}}} - \frac{1}{\xi_{u,p}} x_u^{r_{u,p}-l} e^{-\frac{x_u}{\xi_{u,p}}} \right) dx_u + \frac{\epsilon^{\text{dl}}}{\sigma^{\text{dl}}} \delta[r_{u,p}-l] \\ &\stackrel{(a)}{=} \xi_{u,p}^{r_{u,p}-l-1} (r_{u,p}-l)! e^{\frac{\sigma^{\text{dl}}}{\epsilon^{\text{dl}} \xi_{u,p}}} \left(E_{r_{u,p}-l} \left(\frac{\sigma^{\text{dl}}}{\epsilon^{\text{dl}} \xi_{u,p}} \right) - E_{r_{u,p}-l+1} \left(\frac{\sigma^{\text{dl}}}{\epsilon^{\text{dl}} \xi_{u,p}} \right) \right), \end{aligned} \quad (93)$$

and (a) follows from (91) and the integral formula

$$\begin{aligned} \frac{1}{\xi_{u,p}} e^{\frac{\sigma^{\text{dl}}}{\epsilon^{\text{dl}} \xi_{u,p}}} E_0 \left(\frac{\sigma^{\text{dl}}}{\epsilon^{\text{dl}} \xi_{u,p}} \right) &= \frac{1}{\xi_{u,p}} e^{\frac{\sigma^{\text{dl}}}{\epsilon^{\text{dl}} \xi_{u,p}}} \int_1^\infty e^{-\frac{\sigma^{\text{dl}}}{\epsilon^{\text{dl}} \xi_{u,p}} t} dt \\ &= \frac{\epsilon^{\text{dl}}}{\sigma^{\text{dl}}}. \end{aligned} \quad (94)$$

Substituting the expressions of $\bar{a}_{u,1}$ and $\bar{a}_{u,2}$ into (89) and after some manipulation, we can obtain $\tilde{r}_{\text{mmse}}^{\text{dl,appro}}$ in (44). This completes the proof.

APPENDIX D
PROOF OF THEOREM 3

The analogues of independence and Gaussian distribution in classical probability theory are freeness and semicircular distribution in free probability theory, respectively [59]. We denote

$$\widehat{\mathbf{X}}_k = \begin{pmatrix} \mathbf{0}_{M \times M} & \mathbf{H}_k \\ \mathbf{H}_k^H & \mathbf{0}_{U \times U} \end{pmatrix} \in \mathbb{C}^{(M+U) \times (M+U)}.$$

Furthermore, we define

$$\mathbf{A}_{u,k} = \begin{pmatrix} \mathbf{V}_k & \mathbf{0}_{M \times U} \\ \mathbf{0}_{U \times \tilde{M}} & \mathbf{I}_U \end{pmatrix}, \quad (95)$$

$$\widehat{\mathbf{H}}_k = \begin{pmatrix} \mathbf{0}_{\tilde{M} \times \tilde{M}} & \tilde{\mathbf{H}}_k \\ \tilde{\mathbf{H}}_k^H & \mathbf{0}_{U \times U} \end{pmatrix}, \quad (96)$$

with $\tilde{\mathbf{H}}_k = [\tilde{\mathbf{h}}_{1,k}, \dots, \tilde{\mathbf{h}}_{U,k}] \in \mathbb{C}^{\tilde{M} \times U}$. Then, $\widehat{\mathbf{X}}_k$ can be rewritten as

$$\widehat{\mathbf{X}}_k = \mathbf{A}_k \widehat{\mathbf{H}}_k \mathbf{A}_k^H, \quad (97)$$

We apply the free deterministic equivalent method [28], [59] and replace matrix $\widehat{\mathbf{H}}_k$ consisting of Gaussian entries with matrix $\widehat{\mathcal{H}}_k$, where the entries $[\widehat{\mathcal{H}}_k]_{i,j}$ are circular elements with variance being the same as that of $[\widehat{\mathbf{H}}_k]_{i,j}$, and $\mathbb{E} \{ [\widehat{\mathcal{H}}_k]_{i,j} [\widehat{\mathcal{H}}_k]_{s,v} \} = \mathbb{E} \{ [\widehat{\mathbf{H}}_k]_{i,j} [\widehat{\mathbf{H}}_k]_{s,v} \}$ for $1 \leq i, j, s, v \leq M+U$. The entries on and above the diagonal are free and $[\widehat{\mathcal{H}}_k]_{i,j} = [\widehat{\mathcal{H}}_k]_{j,i}^*$. Then, we have

$$\mathbb{E} \{ \widehat{\mathcal{H}}_k \mathbf{C} \widehat{\mathcal{H}}_k \} = \mathbb{E} \{ \widehat{\mathbf{H}}_k \mathbf{C} \widehat{\mathbf{H}}_k \}. \quad (98)$$

We call

$$\widehat{\mathcal{X}}_k = \mathbf{A}_k \widehat{\mathcal{H}}_k \mathbf{A}_k^H \quad (99)$$

the free deterministic equivalent of $\widehat{\mathbf{X}}_k$. For convenience, we also write $\widehat{\mathbf{X}}_k$ as

$$\widehat{\mathbf{X}}_k = \begin{pmatrix} \mathbf{0}_{M \times M} & \mathbf{H}_k \\ \mathbf{H}_k^H & \mathbf{0}_{U \times U} \end{pmatrix}, \quad (100)$$

where we denote $\mathbf{H}_k \mathbf{H}_k^H$ by \mathbf{B}_k and call \mathbf{B}_k the free deterministic equivalent of \mathbf{B}_k .

Let $\overline{\mathbf{B}}_{k,n} \in \mathbb{C}^{M \times M}$ denote $\mathbb{E}\{\mathbf{B}_k^n\}$, which is also the deterministic equivalent of \mathbf{B}_k^n [29], *i.e.*,

$$\lim_{M \rightarrow \infty} \overline{\mu}_{k,n} - \mathbb{E}\{\mu_{k,n}\} = 0, \quad (101)$$

where $\overline{\mu}_{k,n} = \frac{1}{M} \text{tr}(\overline{\mathbf{B}}_{k,n})$. Furthermore, we can obtain $\overline{\mu}_{k,n}$ from $\overline{\mathbf{B}}_{k,n}$.

The matrix $\widehat{\mathbf{X}}_k$ is semicircular over \mathbb{C} , we have that only the second order operator-valued cumulant $\kappa_2(\widehat{\mathbf{X}}_k \mathbf{C}, \widehat{\mathbf{X}}_k)$ is not a zero matrix [29], defined as

$$\kappa_2(\widehat{\mathbf{X}}_k \mathbf{C}, \widehat{\mathbf{X}}_k) = \mathbb{E}\{\widehat{\mathbf{X}}_k \mathbf{C} \widehat{\mathbf{X}}_k\} = \tilde{\eta}_k(\mathbf{C}). \quad (102)$$

Let $\overline{\mathbf{D}}_{k,n}$ denote $\mathbb{E}\{\widehat{\mathbf{X}}_k^n\}$, and we have the following relation [60]

$$\overline{\mathbf{D}}_{k,2n+2} = \sum_{j=1}^n \tilde{\eta}_k(\overline{\mathbf{D}}_{k,2j}) \overline{\mathbf{D}}_{k,2n-2j}. \quad (103)$$

From the relation between $\widehat{\mathbf{X}}_k^{2n}$ and \mathbf{B}_k^n

$$\widehat{\mathbf{X}}_k^{2n} = \begin{pmatrix} \mathbf{B}_k^n & 0 \\ 0 & (\mathbf{H}_k^H \mathbf{H}_k)^n \end{pmatrix}, \quad (104)$$

we have that

$$\overline{\mathbf{D}}_{k,2n} = \begin{pmatrix} \overline{\mathbf{B}}_{k,n} & 0 & \cdots & 0 \\ 0 & \overline{\psi}_{1,k,n} & \cdots & 0 \\ \vdots & \vdots & \ddots & \vdots \\ 0 & 0 & \cdots & \overline{\psi}_{U,k,n} \end{pmatrix}, \quad (105)$$

which further leads to (61) and (62). The initial values are $\overline{\mathbf{B}}_{k,0} = \mathbf{I}_M$ and $\overline{\psi}_{u,k,n} = 1$ for $1 \leq u \leq U$. This completes the proof.

ACKNOWLEDGMENT

The authors would like to thank the associate editor and the anonymous reviewers for their helpful comments and suggestions

REFERENCES

- [1] X. Yu, A.-A. Lu, X. Q. Gao, G. Y. Li, G. Ding, and C.-X. Wang, "Massive MIMO communication over HF skywave channels," presented at the IEEE GLOBECOM, 2021.
- [2] W. Saad, M. Bennis, and M. Chen, "A vision of 6G wireless systems: Applications, trends, technologies, and open research problems," *IEEE Netw.*, vol. 34, no. 3, pp. 134–142, Oct. 2020.
- [3] L. You, K.-X. Li, J. Wang, X. Gao, X.-G. Xia, and B. Ottersten, "Massive MIMO transmission for LEO satellite communications," *IEEE J. Sel. Areas Commun.*, vol. 38, no. 8, pp. 1851–1865, Aug. 2020.
- [4] M. Uysal and M. Heidarpour, "Cooperative communication techniques for future-generation HF radios," *IEEE Commun. Mag.*, vol. 50, no. 10, pp. 56–63, Oct. 2012.
- [5] J. Wang, G. Ding, and H. Wang, "HF communications: Past, present, and future," *China Commun.*, vol. 15, no. 9, pp. 1–9, Sep. 2018.

- [6] S. D. Gunashekar, E. M. Warrington, and S. Salous, "Investigations into the feasibility of multiple input multiple output techniques within the HF band: Preliminary results," *Radio Sci.*, vol. 44, no. 1, pp. 1–15, Feb. 2009.
- [7] R. C. Daniels and S. W. Peters, "A new MIMO HF data link: Designing for high data rates and backwards compatibility," in *Proc. IEEE Mil. Commun. Conf. (MILCOM)*, San Diego, CA, USA, Nov. 2013, pp. 1256–1261.
- [8] Y. Erhel, D. Lemur, M. Oger, J. Le Masson, and F. Marie, "Evaluation of ionospheric HF MIMO channels: Two complementary circular polarizations reduce correlation," *IEEE Antennas Propag. Mag.*, vol. 58, no. 6, pp. 38–48, Dec. 2016.
- [9] U. Umairah, G. Hendratoro, A. Mauludiyanto, and T. Fukusako, "Capacity of 2×2 MIMO HF NVIS channels with linearly polarized horizontal antennas," *IEEE Wireless Commun. Lett.*, vol. 8, no. 4, pp. 1120–1123, Aug. 2019.
- [10] T. L. Marzetta, E. G. Larsson, H. Yang, and H. Q. Ngo, *Fundamentals Massive MIMO*. Cambridge, U.K.: Cambridge Univ. Press, 2016.
- [11] L. Lu, G. Y. Li, A. L. Swindlehurst, A. Ashikhmin, and R. Zhang, "An overview of massive MIMO: Benefits and challenges," *IEEE J. Sel. Topics Signal Process.*, vol. 8, no. 5, pp. 742–758, Oct. 2014.
- [12] B. Wang, F. Gao, S. Jin, H. Lin, and G. Y. Li, "Spatial- and frequency-wideband effects in millimeter-wave massive MIMO systems," *IEEE Trans. Signal Process.*, vol. 66, no. 13, pp. 3393–3406, Jul. 2018.
- [13] C. Sun, X. Gao, J. Wang, Z. Ding, and X.-G. Xia, "Beam domain massive MIMO for optical wireless communications with transmit lens," *IEEE Trans. Commun.*, vol. 67, no. 3, pp. 2188–2202, Mar. 2019.
- [14] A.-A. Lu, X. Gao, W. Zhong, C. Xiao, and X. Meng, "Robust transmission for massive MIMO downlink with imperfect CSI," *IEEE Trans. Commun.*, vol. 67, no. 8, pp. 5362–5376, Aug. 2019.
- [15] G. J. Frazer, "Experimental results for MIMO methods applied in over-the-horizon radar," *IEEE Aerosp. Electron. Syst. Mag.*, vol. 32, no. 12, pp. 52–69, Dec. 2017.
- [16] C. Watterson, J. Juroshek, and W. Bensema, "Experimental confirmation of an HF channel model," *IEEE Trans. Commun.*, vol. C-18, no. 6, pp. 792–803, Dec. 1970.
- [17] J. F. Mastrangelo, J. J. Lemmon, L. E. Vogler, J. A. Hoffmeyer, L. E. Pratt, and C. J. Behm, "A new wideband high frequency channel simulation system," *IEEE Trans. Commun.*, vol. 45, no. 1, pp. 26–34, Jan. 1997.
- [18] E. E. Johnson, *Third-Generation Wideband HF Radio Communications*. Boston, MA, USA: Artech House, 2013.
- [19] Z. Qin *et al.*, "Link quality analysis based channel selection in high-frequency asynchronous automatic link establishment: A matrix completion approach," *IEEE Syst. J.*, vol. 12, no. 2, pp. 1957–1968, Jun. 2018.
- [20] B. Wang *et al.*, "Spatial-wideband effect in massive MIMO with application in mmWave systems," *IEEE Commun. Mag.*, vol. 56, no. 12, pp. 134–141, Dec. 2018.
- [21] K. Dovelos, M. Matthaiou, H. Q. Ngo, and B. Bellalta, "Channel estimation and hybrid combining for wideband terahertz massive MIMO systems," *IEEE J. Sel. Areas Commun.*, vol. 39, no. 6, pp. 1604–1620, Jun. 2021.
- [22] A. Liao *et al.*, "Terahertz ultra-massive MIMO-based aeronautical communications in space-air-ground integrated networks," *IEEE J. Sel. Areas Commun.*, vol. 39, no. 6, pp. 1741–1767, Jun. 2021.
- [23] J. Nilsson and T. Giles, "Wideband multi-carrier transmission for military HF communication," in *Proc. IEEE MILCOM*, Monterey, QC, USA, vol. 2, Nov. 1997, pp. 1046–1051.
- [24] T. Hwang, C. Yang, G. Wu, S. Li, and G. Y. Li, "OFDM and its wireless applications: A survey," *IEEE Trans. Veh. Technol.*, vol. 58, no. 4, pp. 1673–1694, May 2009.
- [25] F. Rusek *et al.*, "Scaling up MIMO: Opportunities and challenges with very large arrays," *IEEE Signal Process. Mag.*, vol. 30, no. 1, pp. 40–60, Jan. 2013.
- [26] S. Moshavi, "Multi-user detection for DS-CDMA communications," *IEEE Commun. Mag.*, vol. 34, no. 10, pp. 124–136, Oct. 1996.
- [27] A. Kammoun, A. Müller, E. Björnson, and M. Debbah, "Linear precoding based on polynomial expansion: Large-scale multi-cell MIMO systems," *IEEE J. Sel. Topics Signal Process.*, vol. 8, no. 5, pp. 861–875, Oct. 2014.
- [28] R. Speicher and C. Vargas, "Free deterministic equivalents, rectangular random matrix models, and operator-valued free probability theory," *Random Matrices, Theory Appl.*, vol. 1, no. 2, Apr. 2012, Art. no. 1150008.

- [29] A.-A. Lu, X. Gao, Y. R. Zheng, and C. Xiao, "Low complexity polynomial expansion detector with deterministic equivalents of the moments of channel Gram matrix for massive MIMO uplink," *IEEE Trans. Commun.*, vol. 64, no. 2, pp. 586–600, Feb. 2016.
- [30] N. Maslin, *HF Communications: A Systems Approach*. London, U.K.: Pitman, 1987.
- [31] *Testing of HF Modems With Bandwidths of up to About 12 kHz Using Ionospheric Channel Simulators*, document Rec. ITU-R F.1487, 2000. [Online]. Available: <https://www.itu.int/rec/R-REC-F.1487-0-200005-1/en>
- [32] B. Perry, "A new wideband HF technique for MHz-bandwidth spread-spectrum radio communications," *IEEE Commun. Mag.*, vol. CM-21, no. 6, pp. 28–36, Sep. 1983.
- [33] C. Zhou, Z. Zhao, F. Deng, B. Ni, and G. Chen, "Midlatitude ionospheric HF channel reciprocity: Evidence from the ionospheric oblique incidence sounding experiments," *Radio Sci.*, vol. 45, no. 6, pp. 1–18, Dec. 2010.
- [34] R. Shepherd and J. Lomax, "Frequency spread in ionospheric radio propagation," *IEEE Trans. Commun. Technol.*, vol. CT-15, no. 2, pp. 268–275, Apr. 1967.
- [35] *Digital Radio Mondiale (DRM): System Specification*, document ETSI ES 201 980 v4.1.2, 2017. [Online]. Available: <https://www.drm.org>
- [36] S. A. Laraway, H. Moradi, and B. Farhang-Boroujeny, "BER performance study of HF band FB-MC-SS," in *Proc. IEEE Int. Conf. Commun. (ICC)*, Kuala Lumpur, Malaysia, May 2016, pp. 1–7.
- [37] R. D. Hunsucker and H. F. Bates, "Survey of polar and auroral region effects on HF propagation," *Radio Sci.*, vol. 4, no. 4, pp. 347–365, Apr. 1969.
- [38] A. L. Moustakas, G. C. Alexandropoulos, A. Polydoros, I. Kaddas, and I. Dagher, "Impact of imperfect channel estimation in HF OFDM-MIMO communications," in *Proc. IEEE 30th Annu. Int. Symp. Pers., Indoor Mobile Radio Commun. (PIMRC)*, Istanbul, Turkey, Sep. 2019, pp. 1–6.
- [39] H. A. Whale, "The angular spread of radio waves in long-distance ionospheric propagation," *Radio Sci.*, vol. 1, no. 7, pp. 743–750, Jul. 1966.
- [40] P. J. Gething, *Radio Direction Finding and Superresolution*. London, U.K.: IET, 1991.
- [41] P. Kyösti *et al.*, "IST-4-027756 WINNER II D1.1.2 v1.1: WINNER II channel models," EBITG, TUI, UOULU, CU/CRC, NOKIA, Espoo, Finland, Tech. Rep., 2007. [Online]. Available: <http://www.ist-winner.org>
- [42] B. D. Perry and R. Rifkin, "Measured wideband HF mid-latitude channel characteristics," in *Proc. IEEE Mil. Commun. Conf.*, Boston, MA, USA, Oct. 1989, pp. 822–829.
- [43] P. S. Cannon *et al.*, "Damson HF channel characterisation—A review," in *Proc. 21st Century Mil. Commun. Archit. Technol. Inf. Superiority (MILCOM)*, Los Angeles, CA, USA, Oct. 2000, pp. 59–64.
- [44] H. Q. Ngo, E. G. Larsson, and T. L. Marzetta, "Massive MU-MIMO downlink TDD systems with linear precoding and downlink pilots," in *Proc. Allerton Conf. Commun., Control Comput.*, Monticello, IL, USA, Oct. 2013, pp. 293–298.
- [45] V. K. Nguyen and J. S. Evans, "Multiuser transmit beamforming via regularized channel inversion: A large system analysis," in *Proc. IEEE Global Telecommun. Conf. (IEEE GLOBECOM)*, New Orleans, LA, USA, Dec. 2008, pp. 1–4.
- [46] H. Q. Ngo, E. G. Larsson, and T. L. Marzetta, "Energy and spectral efficiency of very large multiuser MIMO systems," *IEEE Trans. Commun.*, vol. 61, no. 4, pp. 1436–1449, Apr. 2013.
- [47] A. Benzin, G. Caire, Y. Shadmi, and A. M. Tulino, "Low-complexity truncated polynomial expansion DL precoders and UL receivers for massive MIMO in correlated channels," *IEEE Trans. Wireless Commun.*, vol. 18, no. 2, pp. 1069–1084, Feb. 2019.
- [48] R. R. Müller and S. Verdú, "Design and analysis of low-complexity interference mitigation on vector channels," *IEEE J. Sel. Areas Commun.*, vol. 19, no. 8, pp. 1429–1441, Aug. 2001.
- [49] R. Hunger, "Floating point operations in matrix-vector calculus," Technische Universität München, Associate Inst. Signal Process., Munich, Germany, Tech. Rep. v1.3, 2007.
- [50] M. Palmese and A. Trucco, "An efficient digital CZT beamforming design for near-field 3-D sonar imaging," *IEEE J. Ocean. Eng.*, vol. 35, no. 3, pp. 584–594, Jul. 2010.
- [51] L. E. Sjöberg and M. Shirazian, "Solving the direct and inverse geodetic problems on the ellipsoid by numerical integration," *J. Surveying Eng.*, vol. 138, no. 1, pp. 9–16, Feb. 2012.
- [52] *Proplab-Pro Version 3*, Solar Terr. Dispatch, Stirling, AB, Canada, 2021. [Online]. Available: <http://www.spacew.com/proplab/index.html>
- [53] K. Davies, *Ionospheric Radio*. London, U.K.: Peregrinus, 1990.
- [54] G. Lane, *Signal-to-Noise Predictions Using VOACAP: A User's Guide*. Cedar Rapids, IA, USA: Rockwell-Collins, 2001.
- [55] L. You *et al.*, "Pilot reuse for massive MIMO transmission over spatially correlated Rayleigh fading channels," *IEEE Trans. Wireless Commun.*, vol. 14, no. 6, pp. 3352–3366, Jun. 2015.
- [56] E. Bjornson *et al.*, "Exploiting quantized channel norm feedback through conditional statistics in arbitrarily correlated MIMO systems," *IEEE Trans. Signal Process.*, vol. 57, no. 10, pp. 4027–4041, Oct. 2009.
- [57] J. Wang, S. Jin, X. Gao, K.-K. Wong, and E. Au, "Statistical eigenmode-based SDMA for two-user downlink," *IEEE Trans. Signal Process.*, vol. 60, no. 10, pp. 5371–5383, Oct. 2012.
- [58] Q. Zhang, S. Jin, K.-K. Wong, H. Zhu, and M. Matthaiou, "Power scaling of uplink massive MIMO systems with arbitrary-rank channel means," *IEEE J. Sel. Topics Signal Process.*, vol. 8, no. 5, pp. 966–981, Oct. 2014.
- [59] A.-A. Lu, X. Q. Gao, and C. Xiao, "Free deterministic equivalents for the analysis of MIMO multiple access channel," *IEEE Trans. Inf. Theory*, vol. 62, no. 8, pp. 4604–4629, Aug. 2016.
- [60] R. Speicher, "Operator-valued free probability and block random matrices," in *Proc. Instruct. Workshop Free Probab.* Chennai, India: IMSc, Jul. 2010, pp. 1–107. [Online]. Available: <https://www.imsc.res.in/~sunder/ovfpbrm.pdf>



Xianglong Yu (Student Member, IEEE) received the B.E. and M.E. degrees in electronic engineering from Xidian University, Xi'an, China, in 2014 and 2017, respectively. He is currently pursuing the Ph.D. degree with the National Mobile Communications Research Laboratory, Southeast University, Nanjing, China. His research interests include massive MIMO communications, HF communications, signal processing, and machine learning for wireless communications.



An-An Lu (Member, IEEE) received the B.E., M.E., and Ph.D. degrees in electronic engineering from Southeast University, Nanjing, China, in 2006, 2012, and 2017, respectively.

From 2006 to 2008, he was with the Research Department, Hejian Technology Company Ltd., Suzhou, China. From November 2014 to February 2016, he visited Missouri University of Science and Technology, Rolla, MO, USA. He is currently a Lecturer with the National Mobile Communications Research Laboratory, Southeast University. His research interests include information theory and wireless communications.



Xiqi Gao (Fellow, IEEE) received the Ph.D. degree in electrical engineering from Southeast University, Nanjing, China, in 1997.

In April 1992, he joined the Department of Radio Engineering, Southeast University. From September 1999 to August 2000, he was a Visiting Scholar at Massachusetts Institute of Technology, Cambridge, and Boston University, Boston, MA, USA. Since May 2001, he has been a Professor of information systems and communications. From August 2007 to July 2008, he visited Darmstadt

University of Technology, Darmstadt, Germany, as a Humboldt Scholar. His current research interests include broadband multicarrier communications, massive MIMO wireless communications, satellite communications, optical wireless communications, information theory, and signal processing for wireless communications.

Dr. Gao received the Science and Technology Awards of the State Education Ministry of China in 1998, 2006, and 2009, the National Technological Invention Award of China in 2011, the Science and Technology Award of Jiangsu Province of China in 2014, and the 2011 IEEE Communications Society Stephen O. Rice Prize Paper Award in the field of communications theory. From 2007 to 2012, he served as an Editor for the IEEE TRANSACTIONS ON WIRELESS COMMUNICATIONS. From 2009 to 2013, he served as an Associate Editor for the IEEE TRANSACTIONS ON SIGNAL PROCESSING. From 2015 to 2017, he served as an Editor for the IEEE TRANSACTIONS ON COMMUNICATIONS.



Guoru Ding (Senior Member, IEEE) received the B.S. degree (Hons.) in electrical engineering from Xidian University, Xi'an, China, in 2008, and the Ph.D. degree (Hons.) in communications and information systems from the College of Communications Engineering, Nanjing, China, in 2014.

From 2015 to 2018, he was a Post-Doctoral Research Associate with the National Mobile Communications Research Laboratory, Southeast University, Nanjing. He is currently a Professor with the College of Communications Engineering, Nanjing.

His research interests include cognitive radio networks, massive MIMO, machine learning, and data analytics over wireless networks. He has received the Excellent Doctoral Thesis Award of the China Institute of Communications in 2016, Alexander von Humboldt Fellowship in 2017, the Excellent Young Scientist of Wuwenjun Artificial Intelligence in 2018, and the 14th IEEE COMSOC Asia-Pacific Outstanding Young Researcher Award in 2019. He was a recipient of the Natural Science Foundation for Distinguished Young Scholars of Jiangsu Province, China, and six best paper awards from international conferences, such as the IEEE VTC-FALL 2014. He has served as a Guest Editor for the IEEE JOURNAL ON SELECTED AREAS IN COMMUNICATIONS Special Issue on Spectrum Sharing and Aggregation in Future Wireless Networks. He is an Associate Editor of the IEEE TRANSACTIONS ON COGNITIVE COMMUNICATIONS AND NETWORKING, an Editor of *China Communications*, and a Guest Editor of *Chinese Journal of Aeronautics*.



Cheng-Xiang Wang (Fellow, IEEE) received the B.Sc. and M.Eng. degrees in communication and information systems from Shandong University, Jinan, China, in 1997 and 2000, respectively, and the Ph.D. degree in wireless communications from Aalborg University, Aalborg, Denmark, in 2004.

He was a Research Assistant with Hamburg University of Technology, Hamburg, Germany, from 2000 to 2001, a Visiting Researcher with Siemens AG Mobile Phones, Munich, Germany, in 2004, and a Research Fellow with the University of Agder,

Grimstad, Norway, from 2001 to 2005. He has been with Heriot-Watt University, Edinburgh, U.K., since 2005, where he was promoted to a Professor in 2011. In 2018, he joined Southeast University, Nanjing, China, as a Professor. He is also a part-time Professor with Purple Mountain Laboratories, Nanjing. He has authored four books, three book chapters, and more than 430 papers in refereed journals and conference proceedings, including 25 highly cited papers. He has also delivered 22 invited keynote speeches/talks and nine tutorials in international conferences. His current research interests include wireless channel measurements and modeling, 6G wireless communication networks, and applying artificial intelligence to wireless communication networks.

Dr. Wang is a member of the Academia Europaea (The Academy of Europe). He is a fellow of IET and China Institute of Communication (CIC). He is a Highly-Cited Researcher recognized by Clarivate Analytics in 2017–2020. He has served as a TPC member, the TPC chair, and the general chair for more than 80 international conferences. He received the 12 Best Paper Awards from IEEE GLOBECOM 2010, IEEE ICCT 2011, ITST 2012, IEEE VTC 2013Spring, IWCMC 2015, IWCMC 2016, IEEE/CIC ICC 2016, WPMC 2016, WOCC 2019, IWCMC 2020, and WCSP 2020. He also received the 2020 and 2021 “AI 2000 Most Influential Scholar Award Honourable Mention” in recognition of his outstanding and vibrant contributions in the field of the Internet of Things. He has served as an Editor for nine international journals, including the IEEE TRANSACTIONS ON WIRELESS COMMUNICATIONS from 2007 to 2009, the IEEE TRANSACTIONS ON VEHICULAR TECHNOLOGY from 2011 to 2017, and the IEEE TRANSACTIONS ON COMMUNICATIONS from 2015 to 2017. He was a Guest Editor of the IEEE JOURNAL ON SELECTED AREAS IN COMMUNICATIONS Special Issue on Vehicular Communications and Networks (a Lead Guest Editor), Special Issue on Spectrum and Energy Efficient Design of Wireless Communication Networks, and Special Issue on Airborne Communication Networks. He was a Guest Editor for the IEEE TRANSACTIONS ON BIG DATA Special Issue on Wireless Big Data. He is an Executive Editorial Committee Member of the IEEE TRANSACTIONS ON WIRELESS COMMUNICATIONS. He is a Guest Editor for the IEEE TRANSACTIONS ON COGNITIVE COMMUNICATIONS AND NETWORKING Special Issue on Intelligent Resource Management for 5G and Beyond. He is an IEEE Communications Society Distinguished Lecturer in 2019 and 2020.



Geoffrey Ye Li (Fellow, IEEE) has been a Chair Professor at Imperial College London, U.K., since 2020. Before moving to Imperial, he was a Professor with Georgia Institute of Technology, USA, for 20 years, and a Principal Technical Staff Member with AT&T Labs—Research in NJ, USA, for five years. His general research interests include statistical signal processing and machine learning for wireless communications. In the related areas, he has published over 600 journals and conference papers in addition to over 40 granted patents and several

books. His publications have been cited around 50,000 times with H-index 100 and he has been recognized as a Highly Cited Researcher, by Thomson Reuters, almost every year.

Dr. Ye Li was awarded as an IEEE Fellow for his contributions to signal processing for wireless communications in 2005. He won several prestigious awards from IEEE Signal Processing Society (Donald G. Fink Overview Paper Award in 2017), IEEE Vehicular Technology Society (James Evans Avant Garde Award in 2013 and Jack Neubauer Memorial Award in 2014), and IEEE Communications Society (Stephen O. Rice Prize Paper Award in 2013, Award for Advances in Communication in 2017, and Edwin Howard Armstrong Achievement Award in 2019). He also received the 2015 Distinguished ECE Faculty Achievement Award from Georgia Tech. He has organized and chaired many international conferences, including the Technical Program Vice-Chair of the IEEE ICC'03 and the General Co-Chair of the IEEE GlobalSIP'14, the IEEE VTC'19 (Fall), and the IEEE SPAWC'20. He has been involved in editorial activities for over 20 technical journals, including the Founding Editor-in-Chief of IEEE JOURNAL ON SELECTED AREAS IN COMMUNICATIONS Special Series on ML in Communications and Networking.